High-Resolution Wind Resource Data Set of the Greater Puerto Rico Region

Manajit Sengupta, Jaemo Yang, and Yu Xie

National Renewable Energy Laboratory

NREL is a national laboratory of the U.S. Department of Energy
Office of Energy Efficiency & Renewable Energy
Operated by the Alliance for Sustainable Energy, LLC

This report is available at no cost from the National Renewable Energy Laboratory (NREL) at www.nrel.gov/publications.

Contract No. DE-AC36-08GO28308

Technical Report
NREL/TP-5D00-84223
December 2022

High-Resolution Wind Resource Data Set of the Greater Puerto Rico Region

Manajit Sengupta, Jaemo Yang, and Yu Xie

National Renewable Energy Laboratory

Suggested Citation
Sengupta, Manajit, Jaemo Yang, and Yu Xie. 2022. *High-Resolution Wind Resource Data Set of the Greater Puerto Rico Region*. Golden, CO: National Renewable Energy Laboratory. NREL/TP-5D00-84223. https://www.nrel.gov/docs/fy23osti/84223.pdf.

NREL is a national laboratory of the U.S. Department of Energy
Office of Energy Efficiency & Renewable Energy
Operated by the Alliance for Sustainable Energy, LLC

This report is available at no cost from the National Renewable Energy Laboratory (NREL) at www.nrel.gov/publications.

Contract No. DE-AC36-08GO28308

Technical Report
NREL/TP-5D00-84223
December 2022

National Renewable Energy Laboratory
15013 Denver West Parkway
Golden, CO 80401
303-275-3000 • www.nrel.gov

NOTICE

This work was authored by the National Renewable Energy Laboratory, operated by Alliance for Sustainable Energy, LLC, for the U.S. Department of Energy (DOE) under Contract No. DE-AC36-08GO28308. Funding provided by U.S. Department of Energy Office of Electricity. The views expressed herein do not necessarily represent the views of the DOE or the U.S. Government.

Cover Photos by Dennis Schroeder: (clockwise, left to right) NREL 51934, NREL 45897, NREL 42160, NREL 45891, NREL 48097, NREL 46526.

Acknowledgments

This work was authored by the National Renewable Energy Laboratory (NREL) for the U.S. Department of Energy (DOE) under Contract No. HSFE02-20-IRWA-0011. Funding was provided by U.S. Federal Emergency Management Agency and performed under the technical management of the Department of Energy Office of Electricity. The views expressed in the article do not necessarily represent the views of the DOE, the Federal Emergency Management Agency (FEMA) or the U.S. Government. The U.S. Government retains and the publisher, by accepting the article for publication, acknowledges that the U.S. Government retains a nonexclusive, paid-up, irrevocable, worldwide license to publish or reproduce the published form of this work, or allow others to do so, for U.S. Government purposes.

The authors acknowledge Marisol Bonnet and Ernesto A. Rivera-Umpierre, Esq., from the U.S. DOE, for their support of this project. The authors also acknowledge Dr. Michael Rossol, from NREL (now with Apeel), for providing technical assistance on the Wind Integration National Dataset (WIND) Toolkit postprocessing for Weather Research and Forecasting (WRF) model outputs; and Dr. Caroline Draxl, Dr. Nicola Bodini, and Dr. Alex Rybchuk, also from NREL, for their valuable advice and feedback for the WRF configuration in producing wind resource data sets. The authors thank Dr. Hyeyum (Hailey) Shin, from the National Center for Atmospheric Research, for her efforts on reviewing this report and providing valuable feedback for modeled wind speed from the WRF planetary boundary layer scheme. Finally, we thank Haiku Sky and Patrick Duffy, from NREL, for the data management and their efforts on conversations with technical stakeholders for the wind resource data sets produced in this project.

List of Acronyms

BouLac	Bougeault and Lacarrere
CAM	Community Atmosphere Model
DOE	U.S. Department of Energy
ERA5	ECMWF Reanalysis Version 5
FARMS	Fast All-sky Radiation Model for Solar applications
FNL	National Centers for Environmental Prediction Final Operational Global Analysis
GOES	Geostationary Operational Environmental Satellites
LBW	land-based wind
LSM	Land Surface Model
MAE	mean absolute error
MBE	mean bias error
MERRA-2	Modern-Era Retrospective analysis for Research and Applications, Version 2
MM5	Mesoscale Model Version 5
MYNN	Mellor–Yamada–Nakanishi–Niino
NDBC	National Data Buoy Center
NREL	National Renewable Energy Laboratory
NSRDB	National Solar Radiation Database
NWP	numerical weather prediction
OSCAT	OceanSat-2 scatterometer
OSW	offshore wind
PBL	planetary boundary layer
PR100	Puerto Rico Grid Resilience and Transition to 100% Renewable Energy Study
reV	Renewable Energy Potential
RMSE	root mean square error
RRTMG	Rapid Radiative Transfer Model for General circulation models
SAM	System Advisor Model
SH	Shin-Hong
TKE	turbulent kinetic energy
WIND Toolkit	Wind Integration National Dataset Toolkit
WMO	World Meteorological Organization
WRF	Weather Research and Forecasting
YSU	Yonsei University

Executive Summary

In February 2022, the U.S. Department of Energy and six national laboratories launched the Puerto Rico Grid Resilience and Transition to 100% Renewable Energy Study (PR100) in partnership with the Federal Emergency Management Agency (FEMA). PR100 aims to provide a comprehensive analysis of possible pathways for Puerto Rico's energy future, with a goal of 100% renewable energy by 2050. As part of the renewable energy potential assessment in this project, we developed 20 years (2001–2020) of data using a numerical weather prediction (NWP) model for land-based wind (LBW) and offshore wind (OSW) resource assessments for Puerto Rico. The research steps in developing the long-term wind resource data sets based on the NWP model were:

1. Model the wind resource based on the Weather Research and Forecasting (WRF) model.
2. Develop WRF model configurations for Puerto Rico.
3. Test the WRF with 11 different physics parameterizations for the planetary boundary layer (PBL).
4. Assess the WRF output from the different PBL schemes against observations.
5. Select a final model configuration that can produce the modeled wind speed with sufficient accuracy.
6. Produce 20 years of wind resource data for the Puerto Rico region.

In the first stage of our framework for developing the wind resource data, we developed a WRF model configuration using two nested domains (9 km and 3 km) to cover Puerto Rico and the U.S. Virgin Islands and to downscale the ERA5 reanalysis data (0.25°×0.25°; hourly interval), developed by the European Centre for Medium-Range Weather Forecasts, to a 3-km domain. For the second stage, we implemented 1-year simulations focused on using 11 different PBL physics parameterizations to find a combination of WRF physics parameterizations that could provide accurately modeled wind speed for Puerto Rico. We also analyzed the sensitivity of the modeled wind speed to PBL schemes for LBW and OSW locations. The WRF output resulting from the 11 WRF experiments using different PBL parameterizations were evaluated against observations obtained from the National Data Buoy Center as well as at hub height for a location for which measurements were available. A final model setup selected through the validation with observational data was used to produce 20 years of data with 3-km spatial and 5-minute temporal resolution. The WRF model output was postprocessed to include wind profiles and basic atmospheric variables in a format that can be easily used for downstream modeling. The wind resource data served as the basis for the wind energy cost analysis for Puerto Rico (Duffy et al. 2022). The 20 years of wind resource data will be made available through the National Renewable Energy Laboratory and will support wind energy development considerations for the PR100 study.

Table of Contents

List of Figures

List of Tables

1 Introduction

In September 2017, hurricanes Irma and Maria swept across Puerto Rico in short succession, leading to the long-term failure of the centralized power grid, which is primarily based on fossil fuels, and thus widespread power outages for more than 6 months (DOE 2018; Lu and Alcantara 2017). The energy crisis severely affected access to clean water, communication systems, transportation, and other essentials of daily life for millions of people. The disaster recovery efforts have created an expansion in distributed generation from renewable energy that is potentially economically viable and could improve energy resilience. The Puerto Rico Energy Public Policy Act, Act 17 of 2019, established the energy goals to reach 100% compliance with the renewable portfolio standard by the year 2050, along with realizing interim goals of 40% by 2025, 60% by 2040, and the phaseout of coal-fired power by 2028. To meet these goals, the government of Puerto Rico and renewable energy developers must establish a comprehensive understanding of the renewable energy resources throughout the greater Puerto Rico region, including high-resolution solar radiation resource mapping on the land surface and land-based wind (LBW) and offshore wind (OSW) resource mapping using at least 10 years of data to account for variability.

The solar energy resource can be inferred from satellite observations in the visible and infrared bands. The National Solar Radiation Database (NSRDB) uses cloud products based on observations from the Geostationary Operational Environmental Satellites (GOES) to compute surface global horizontal irradiance, direct normal irradiance, and diffuse horizontal irradiance (Sengupta et al. 2018). The cloud products as well as the ancillary data from the National Aeronautics and Space Administration's Modern-Era Retrospective analysis for Research and Applications, Version 2 (MERRA-2), are input into the Fast All-sky Radiation Model for Solar applications (FARMS) to produce high-resolution solar radiation data over the United States of America, including the Puerto Rico region (Xie, Sengupta, and Dudhia 2016). With an advanced radiative transfer model to compute solar radiances, users of the solar resource data can also obtain the plane-of-array irradiances for specific photovoltaic orientations at up to 2002 wavelengths from 0.28 μm to 4.0 μm (Xie and Sengupta, 2018; Xie, Sengupta, and Wang 2019).

In general, geostationary or polar-orbiting satellite instruments that can sense clouds are unable to sense wind at various heights in the atmosphere; therefore, the estimation of the wind energy resource based on satellite observations is complicated, restricted, and often more uncertain than the solar resource. Current efforts use a satellite-based synthetic aperture radar or a scatterometer that emits microwave radiation and receives reflections from the ocean surface. Because microwave bands are sensitive to ocean surface roughness generated by surface wind, an empirical relationship between the backscattered microwave signal and ocean wind speed can be developed and used to retrieve OSW speed. A few OSW resource data sets are currently available from the European Space Agency's European Remote Sensing satellite ERS-2 synthetic aperture radar (Hasager et al. 2005), Environment Satellite (Envisat) advanced synthetic aperture radar (Christiansen et al. 2006), and OceanSat-2 scatterometer (OSCAT) (Gadad and Deka 2016).

The numerical weather prediction (NWP) models are useful alternates of the satellite remote sensing techniques to provide large-scale wind energy resource data for both land-based and

offshore scenarios (Al-Yahyai, Charabi, and Gastli 2012; Dvorak, Archer, and Jacobson 2009). Although the accuracy of wind modeling is restricted by the quality of the initial conditions, the physical parameterizations in the NWP model, and the computing capabilities, NWP models are capable of providing larger domain coverages with better spatial resolution, especially in the vertical direction. Numerous studies have developed wind energy resource data using NWP models (Al-Yahyai, Charabi, and Gastli 2012). Dvorak, Archer, and Jacobson (2009) used the Mesoscale Model Version 5 (MM5) to create a wind resource data set in California at a modern wind turbine hub height of 80 m. The 1.67-km and 5-km horizontal resolution data sets were validated using high-resolution bathymetry data. Draxl et al. (2015) used the Weather Research and Forecasting (WRF) model to create the Wind Integration National Dataset (WIND) Toolkit that covers 2-km grids over the continental United Sates at a 5-min resolution. Based on a sensitivity study of wind simulation to NWP physical schemes, the Noah Land Surface Model (LSM) (Niu et al. 2011), the Yonsei University (YSU) boundary-layer scheme (Hong, Noh, and Dudhia 2006), and the parameterization of topographic wind enhancement (Jimenez and Dudhia 2012) were employed. The wind speed, direction, and air temperature are given at the heights of 10 m, 40 m, 60 m, 80 m, 100 m, 120 m, 140 m, 160 m, and 200 m.

In this report, we extended the study of the WIND Toolkit to develop a long-term wind resource data set using the WRF model. In contrast to the WIND Toolkit, which covers the continental United States, we focus on high-resolution grids in a much smaller domain over the greater Puerto Rico region. Consequently, we explore and apply the physical parameterization schemes in the WRF model specifically for the region. Compared to the WIND Toolkit, which seeks a good overall accuracy over a large area, this setup ensures a better opportunity for optimal model performance in the Puerto Rico region. This report is organized as follows: In Part 2, we briefly introduce the WRF model and the model configuration for the greater Puerto Rico region. In Part 3, we report the results from a sensitivity study of wind simulation using various NWP physical schemes. The physical parameterization schemes were tested using surface observations that were primarily selected because of their long-term availability in the greater Puerto Rico region. In Part 4, we report on the development of high-resolution data for the LBW and OSW resource using the WRF model. An analysis of the long-term wind data was conducted and is also discussed.

2 Modeling the Wind Resource

2.1 Modeling Approach

The primary model used in this project is the WRF model, a publicly available NWP model distributed by the National Center for Atmospheric Research. The National Renewable Energy Laboratory (NREL) has been instrumental in augmenting this model to develop additional capabilities to improve solar and wind forecasts through work funded by the U.S. Department of Energy (Jimenez et al. 2022; Kim et al. 2021; Sengupta et al. 2022; Xie et al. 2020; Xie et al. 2022; Yang et al. 2021; Yang et al. 2022). For Puerto Rico, we used the WRF model, Version 4.3 (Skamarock et al. 2019) and produced 3-km wind resource data sets to cover the period from 2001–2020. WRF was used to develop wind speed and direction at various hub heights as well as additional variables required for wind energy modeling.

2.2 WRF Configuration for Puerto Rico

As a first step, we developed a WRF grid covering Puerto Rico and the U.S. Virgin Islands. WRF is configured with two nests, with the outer grid having a horizontal grid spacing of 9 km and the inner nest having a grid spacing of 3 km (Figure 1). The 3-km domain is the focus area of this project. We used 61 vertical levels for both domains. The 9-km outer domain was designed to be relatively large to capture the motion of tropical cyclones.

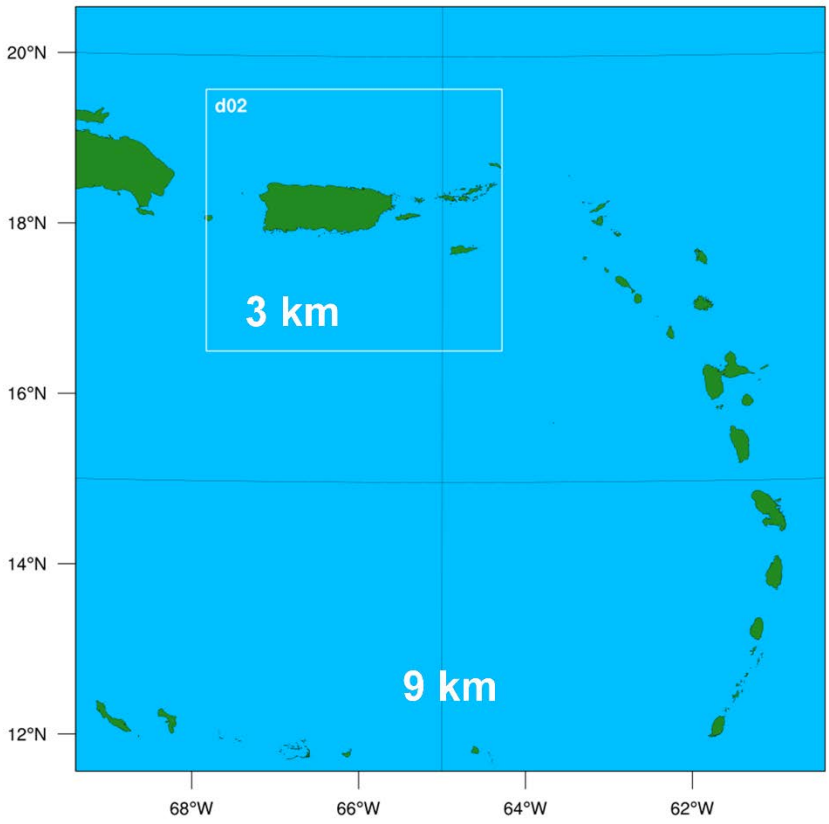

Figure 1. WRF domain for the greater Puerto Rico region

We used the ERA5 reanalysis data (0.25°×0.25°; hourly interval), developed by the European Centre for Medium-Range Weather Forecasts (Hersbach et al. 2020), for the initial and boundary conditions for the WRF model. The ERA5 data are widely used in the wind industry for wind resource assessment. The data have 30-km horizontal grid spacing and provide various hourly estimates for atmospheric, land, and oceanic climate variables. ERA5 was used in preference to other global analysis or reanalysis data sets because there were some limitations in the others. For example, the National Centers for Environmental Prediction Final (FNL) analysis product (https://rda.ucar.edu/datasets/ds083.2/) provides coarser resolution data (i.e., 6-hourly analysis at a 1°×1° grid), which would have resulted in more uncertainty in the results. Similarly, MERRA-2) (Gelaro et al. 2017), can provide hourly data, but it also has a coarser spatial resolution (0.5°×0.625°) than ERA5. In addition, Optis et al. (2020) compared the ERA5 and MERRA-2 data sets in simulating wind speeds for California. This previous study showed that ERA5 produces better results (reduced error and bias) than MERRA-2 in simulating wind speeds from the WRF model.

The WRF configuration used for this work is summarized in Table 1. Most of the basic settings and physics options were selected based on Optis et al. (2020), except the planetary boundary layer (PBL) and surface layer schemes. The Ferrier scheme (Ferrier et al. 2002) was employed to account for the cloud microphysical processes. For the radiative transfer model, the Rapid Radiative Transfer Model for General circulation models (RRTMG) (Clough et al. 2005; Mlawer et al. 1997) was used to compute shortwave and longwave radiation. The Kain-Fritsch parameterization (Kain 2004) was used to represent cumulus convection for the outer domain (9 km). For the PBL and surface layer schemes, various physics parameterizations were tested (Table 2), and the Shin-Hong (Shin and Hong 2015) and the revised MM5 Monin-Obukhov (Jiménez et al., 2012) schemes were selected to simulate the 20-year wind resource data sets. Finally, the Noah LSM (Chen and Dudhia 2001) was used to account for the land surface interactions.

Table 1. WRF Configuration

Feature	Specification
WRF version	4.3
Grid structure (two grids)	Grid spacing (dx): 9 km (outer), 3 km (inner)
Nesting	Two-way nesting
Vertical levels	61
Model inputs for initial and boundary conditions	ERA5 reanalysis
Atmospheric nudging	Spectral nudging on 9-km domain, applied every 6 hours
Temporal resolution of 2nd domain outputs	5 minutes
SST update	Hourly
Microphysics	Ferrier
Shortwave radiation	RRTMG
Longwave radiation	RRTMG
Cumulus scheme	Kain-Fritsch scheme for 1st domain
PBL scheme	See PBL schemes used for sensitivity analysis (Table 2). Final selection: Shin-Hong
Surface layer scheme	See surface layer schemes used for sensitivity analysis (Table 2). Final selection: Revised MM5 Monin-Obukhov scheme
Land surface model	Noah LSM

2.3 WRF Simulations

To efficiently perform WRF simulations on high-performance computing resources, we ran WRF simulations for each month and stitched 12 sets of 1-month simulations in a postprocessing step to produce a consecutive year of data. We followed the WIND Toolkit and Optis et al. (2020) to set a sufficient spin-up time for the model stabilization. The first 2 days were regarded as the model's spin-up time, and an additional day was added to the tail of the 1-month simulation period. For example, we used 0000 UTC 12/30/2019 and 0000 UTC 02/02/2020 as the start and end times, respectively, to run the January 2020 simulation.

Another important requirement when producing long-term wind resource data is to maintain consistent accuracy when running the monthly simulations. To enable this, one available nudging technique, "spectral nudging," was applied when running the WRF model. The spectral nudging technique allows regional NWP models to generate their own local features and prevents the models from departing from their boundary conditions (Miguez-Macho, Stenchikov, and Robock 2005; Miguez-Macho, Stenchikov, and Robock 2004); however, to avoid excessive reduction in the model's internal variability, we applied spectral nudging only to the outer domain (9 km). To apply the nudging technique in the WRF model, we referred to the parameters related to the spectral nudging that were used in Optis et al. (2020). Note that we explicitly defined the

parameter “gfdda_end_h” in the WRF namelist to be sure that the nudging was applied to the entire 1-month simulation period. Additionally, in this project, an appropriate wave number for the Puerto Rico domain was calculated using an equation (Gómez and Miguez-Macho 2017) that combines grid spacing, number of grid points, and Rossby radius.

3 Development and Validation of the Wind Resource Data Set

3.1 Sensitivity of Modeled Wind Speed Using Various Physics Schemes from WRF

The WRF has various physics options, and results can change depending on the options selected from the list. We implemented WRF runs with various physics schemes for a 1-year simulation period. This was an essential step prior to running multiyear simulations because we needed to find an appropriate WRF configuration that can provide accurate modeled wind resources over Puerto Rico.

Among the various atmospheric physics schemes in the WRF model, the PBL physics is the core process in simulating wind speed near the surface. The PBL is the lowest part of the atmosphere, and surface-atmosphere interactions with turbulent exchanges of mass, momentum, and energy strongly occur within the PBL (Coantic and Seguin 1971); therefore, the PBL physics schemes significantly affect the NWP-modeled wind speeds within the PBL. Recent studies (Hahmann et al. 2015; Olsen et al. 2017; Siuta, West, and Stull 2017; Zhang et al. 2021) have also demonstrated the sensitivity of the modeled wind speed using NWP to different PBL physics schemes.

In this project, we performed 1-year simulations covering 2019 with 11 different PBL parameterizations available in the WRF model (Table 2). The Noah LSM (Chen and Dudhia 2001) was used to represent the land surface for all experiments. As specific PBL schemes only work with relevant surface layer schemes, so we used different surface layer parameterizations that are relevant for each experiment. Key features of the PBL parameterizations are described in Zhang et al. (2021).

Table 2. PBL, LSM, and PBL Schemes Used for 11 Experiments for 1-Year WRF Simulations

Experiment #	PBL	LSM	Surface Layer
E01	MYNN[a] 2.5 level	Noah LSM	MYNN surface layer
E02	YSU	Noah LSM	Revised MM5 Monin-Obukhov scheme
E03	MYJ[b] TKE[c]	Noah LSM	Monin-Obukhov (Janjic) scheme
E04	Eddy-diffusivity mass flux, quasi-normal scale elimination PBL	Noah LSM	QNSE[d] surface layer
E05	MYNN 3rd level	Noah LSM	MYNN surface layer
E06	ACM2[e] (Pleim) PBL	Noah LSM	Pleim-Xiu surface layer
E07	BouLac[f] PBL	Noah LSM	Monin-Obukhov (Janjic) scheme
E08	University of Washington boundary layer scheme from CAM5[g]	Noah LSM	MYNN surface layer
E09	Shin-Hong scale-aware PBL scheme	Noah LSM	Revised MM5 Monin-Obukhov scheme
E10	Grenier-Bretherton-McCaa scheme	Noah LSM	Revised MM5 Monin-Obukhov scheme
E11	TKE+TKE dissipation rate (epsilon) scheme	Noah LSM	MYNN surface layer

[a] MYNN: Mellor–Yamada–Nakanishi–Niino
[b] Mellor–Yamada–Janjić
[c] Turbulent kinetic energy
[d] Quasi-Normal Scale Elimination
[e] Asymmetric Convection Model 2
[f] Bougeault and Lacarrere
[g] Community Atmosphere Model 5

To more specifically analyze the wind resource data in the greater Puerto Rico region, we selected four OSW sites—one each in the northeast, southeast, west, and northwest of the island of Puerto Rico (Figure 2). In addition, four LBW sites were selected—one each in the northeast, southeast, southwest, and northwest of the island.

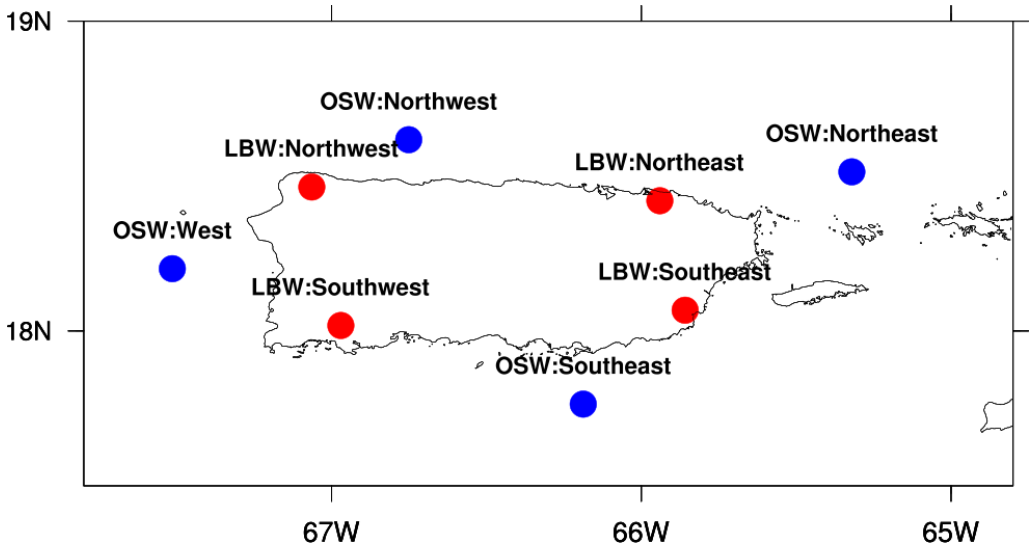

Figure 2. Eight sites for the OSW and LBW resource analysis

Figure 3 and Figure 4 display the monthly mean wind speeds at 160 m from 11 WRF experiments (for the year 2019) for the offshore and land-based sites, respectively. For both OSW and LBW, the WRF experiments focused on using 11 PBL schemes that produce different wind speeds across all seasons. All 11 members show consistent seasonal patterns of OSW and LBW, especially lower wind speeds that are more prevalent in fall than the other seasons for Puerto Rico. For OSW, the difference between the members is smaller in the southeast than the other locations. For this location, the distinguishable modeled winds are not driven by the WRF model even if different PBL parameterizations are used. Some members show notable low wind speeds for OSW and LBW. For example, E07, which was produced using the Bougeault and Lacarrere (BouLac) PBL, exhibits lower wind speeds than the other PBL parameterizations for OSW in the northwest and west (Figure 3), and this pattern is pronounced for LBW (Figure 4).

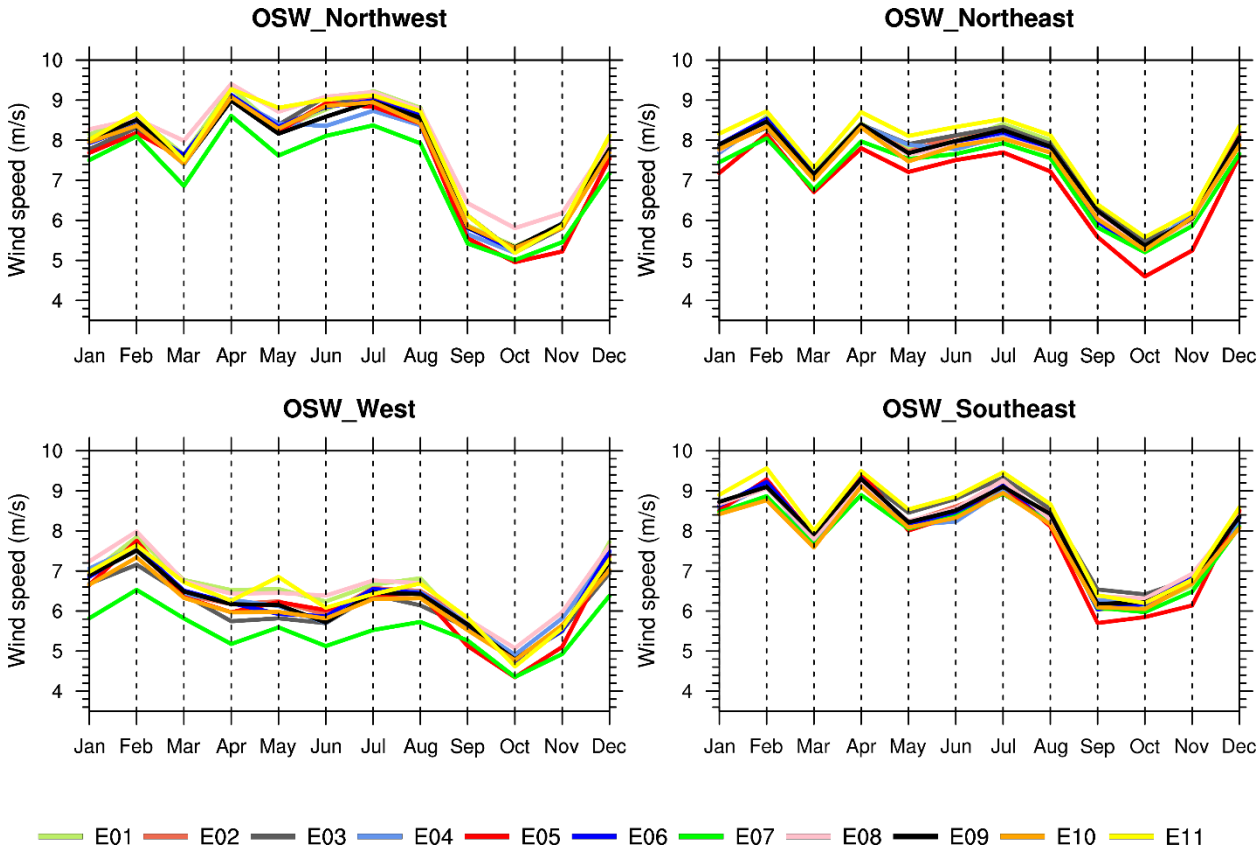

Figure 3. Monthly mean OSW at 160 m from 11 WRF experiments (2019)

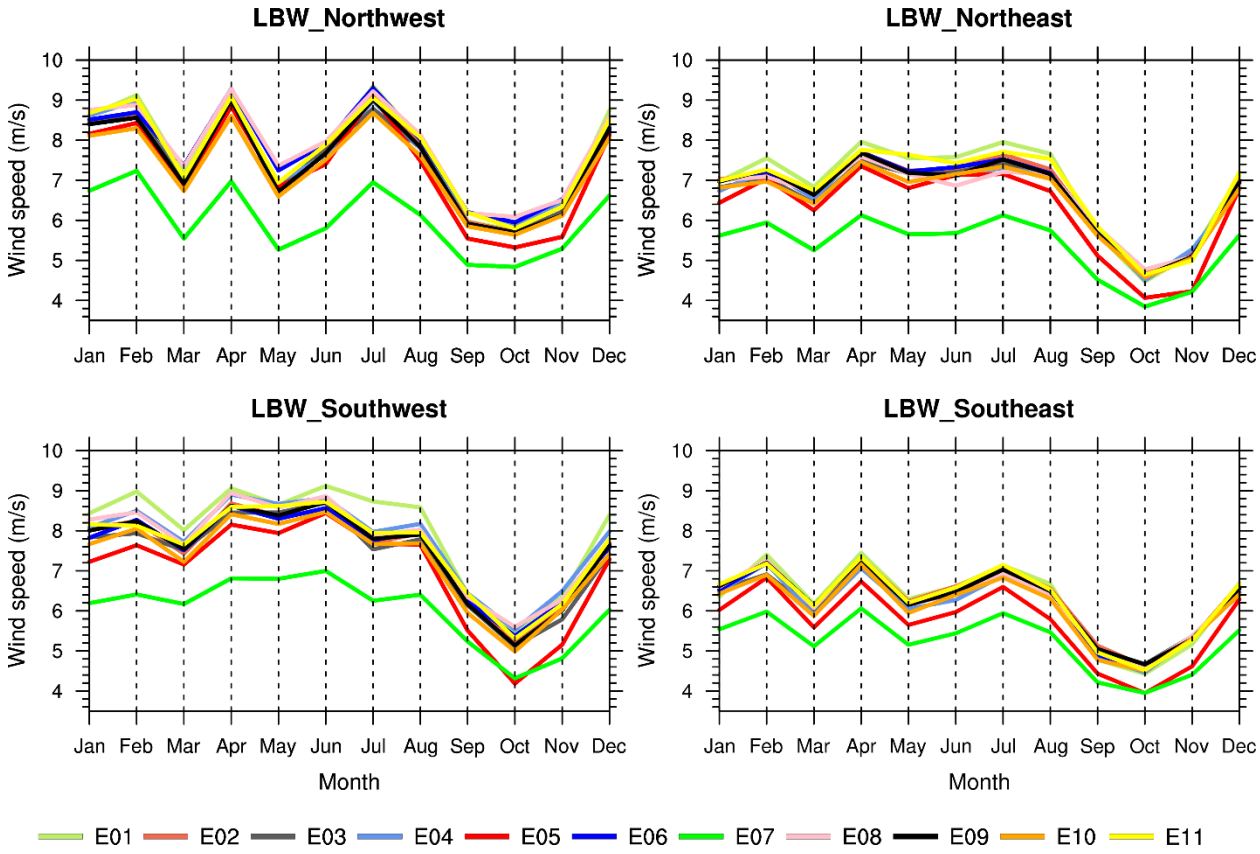

Figure 4. Monthly mean LBW at 160 m from 11 WRF experiments (2019)

Figure 5 displays the hourly mean wind speeds at 160 m from 11 WRF experiments (2019) for the offshore and land-based sites, respectively. Consistent with the results shown in Figure 3, the OSW in the southeast shows a small difference between the members across all hours. The spread in OSW members is larger for the northwest and west than for the northeast and southeast locations. The difference between the members is pronounced for the LBW sites, which indicates that the modeled LBW is sensitive to PBL physics from the WRF model. For the LBW sites, the difference between the LBW members is large during the daytime, and the southwest site also exhibits a large ensemble spread during the nighttime. E07 exhibits lower wind speeds than the other WRF experiments for both OSW and LBW. Especially for LBW sites, E07 behaves differently, with low wind speeds across all hours. In this case, there is a need to check the wind profiles from the experiments for the LBW sites.

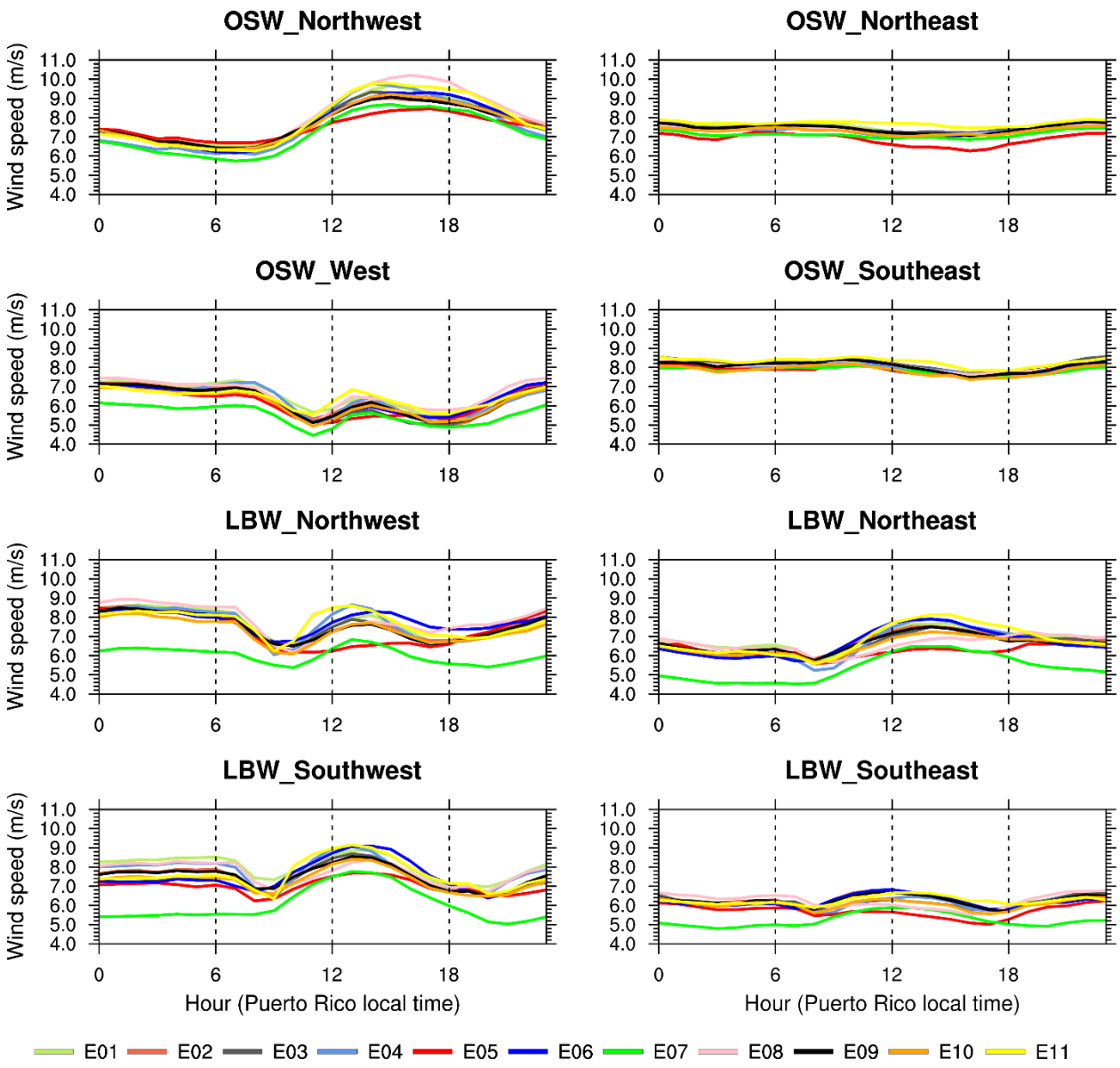

Figure 5. Hourly mean LBW at 160 m from 11 WRF experiments (2019)

Figure 6 and Figure 7 display the annual mean OSW and LBW profiles from 11 WRF experiments for the year 2019. Consistent with the results shown in Figure 3 and Figure 4, the difference between the members is smaller for the southeast site than for the other sites (Figure 6). Given the results from the WRF experiments, the uncertainty of the modeled wind speeds driven by 11 different PBL schemes is lower for the southeast OSW site than the other locations. As shown in Figure 3 and Figure 4, E07 produces low wind speeds across most heights for the northwest and west sites (Figure 6). This tendency of E07 appears in sites for LBW (Figure 7); thus, the PBL scheme used in E07 (BouLac PBL) is not recommended for modeling wind speeds for Puerto Rico. For both LBW and OSW sites, the magnitudes of wind speeds resulting from the 11 PBL schemes do not change at a consistent rate with height. This implies that a PBL scheme producing the lowest wind speeds at the surface level does not always produce the lowest wind speeds at hub height. In addition, the LBW site in the southwest shows a large spread of the 11 members when the height increases (Figure 7). Because the PBL scheme can have a large impact

on the hub-height wind resource in some regions, there is a need to validate the modeled wind speeds at hub height to complement the surface-level validation.

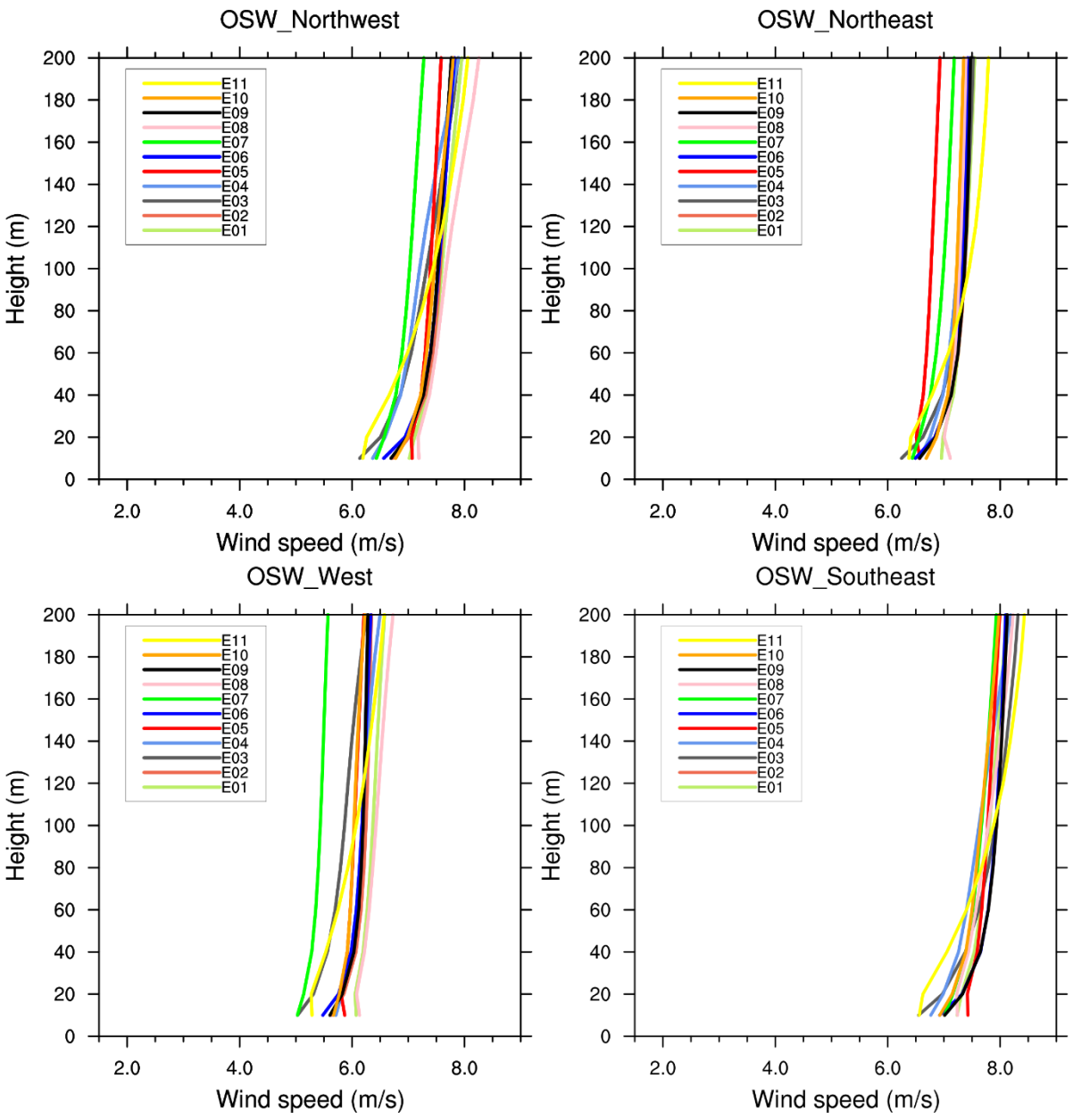

Figure 6. Mean wind profiles from 11 WRF experiments for the OSW sites (2019)

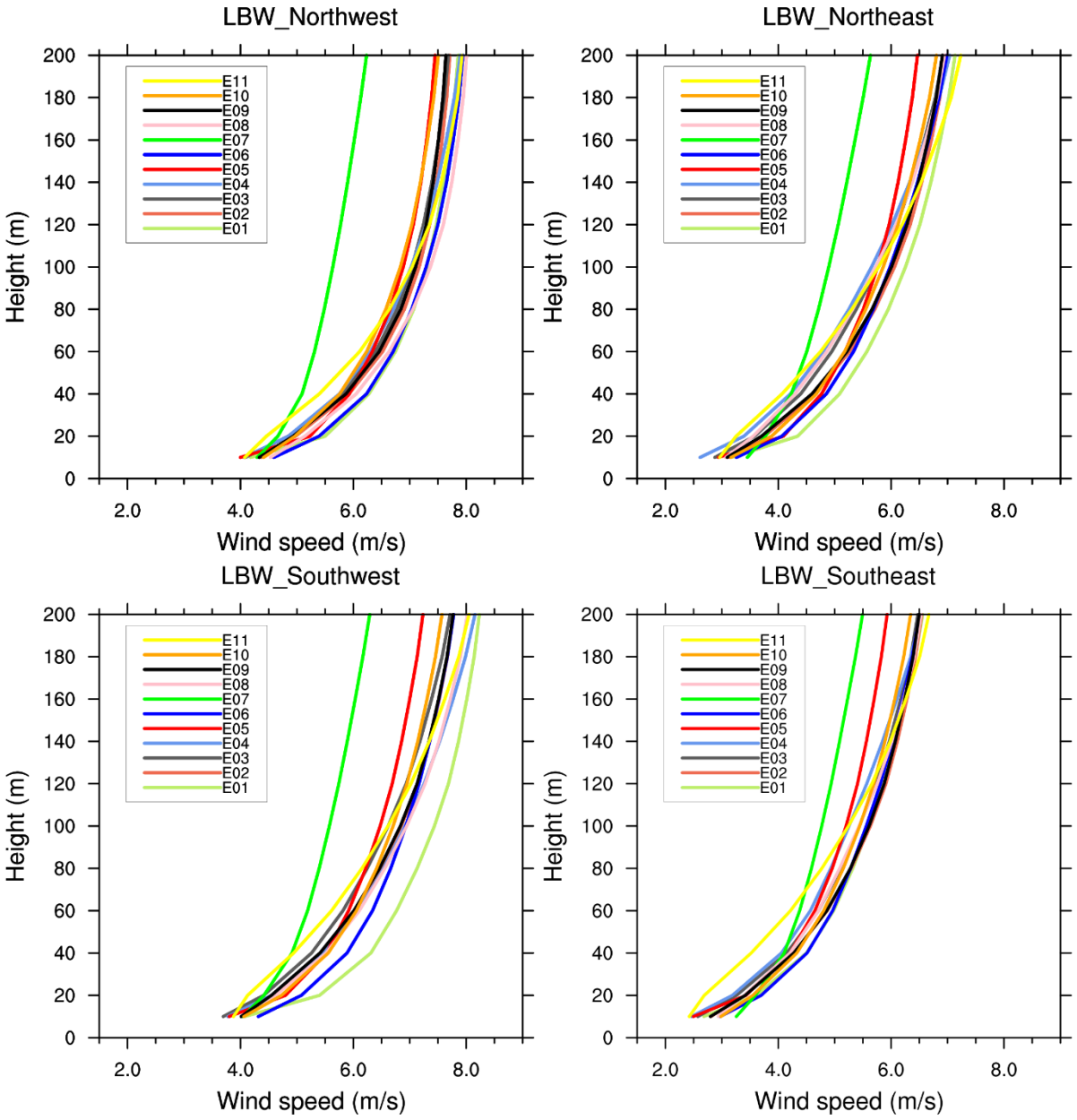

Figure 7. Mean wind profiles from 11 WRF experiments for the LBW sites (2019)

3.2 Selection of a Final Model Setup

To select a final combination of WRF physics, we evaluated 11 WRF simulations using various PBL schemes against observations obtained from the National Data Buoy Center (NDBC) (https://www.ndbc.noaa.gov/). For 2019, the observations were available for seven stations (Figure 8). To evaluate the modeled and observed wind speed at the same height, we vertically interpolated the 10-m wind speed from the WRF model to the anemometer of each station. Because of the small difference between 10 m (modeled wind speed height) and anemometer height, we used a simple method known as the logarithmic wind profile law (Bañuelos-Ruedas et al. 2011) to vertically interpolate the WRF's 10-m wind speed.

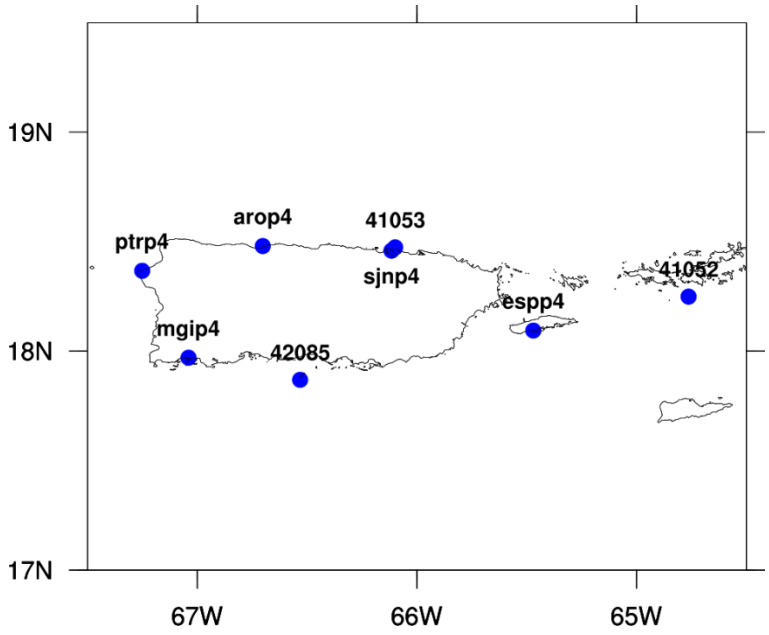

Figure 8. Available NDBC stations for 2019

Four statistical metrics were used for the evaluation of the modeled wind speed against the NDBC observations—root mean square error (RMSE), mean absolute error (MAE), and mean bias error (MBE)—which are determined as follows:

$$RMSE\ (m/s) = \left[\frac{1}{N}\sum_{N}(X-O)^2\right]^{1/2} \tag{3.1}$$

$$MAE\ (m/s) = \frac{1}{N}\sum_{N}|X-O| \tag{3.2}$$

$$MBE\ (m/s) = \frac{1}{N}\sum_{N}(X-O) \tag{3.3}$$

where the observed wind speed is denoted by O, the modeled wind speed is represented by X, and N is the total number of data pairs.

When analyzing the observed-modeled pairs, we classified the observed wind speed into four wind categories—including light breeze (Group 1), moderate breeze (Group 2), strong breeze (Group 3), and gale/storm (Group 4) —following the World Meteorological Organization classification (Table 3). For the evaluation of the WRF wind speed, we focused on the wind speed in Group 2 to consider the range of cut-in and rated wind speed.

Table 3. Wind Speed Classification Used for Model Evaluation

Source: National Oceanic and Atmospheric Administration, Beaufort wind scale, http://www.spc.noaa.gov/faq/tornado/beaufort.html

Group	Range of Observed Wind Speed (m/s)	Classification in This Work	Actual World Meteorological Organization Classification
1	0 < wind speed ≤ 3.1	Light breeze	Calm/light air/light breeze
2	3.1 < wind speed ≤ 8.2	Moderate breeze	Gentle breeze/moderate breeze
3	8.2 < wind speed ≤ 13.9	Strong breeze	Fresh breeze/strong breeze
4	13.9 < wind speed	Gale/storm	Near gale/gale/strong gale/storm

Figure 9 shows the RMSE, MAE, and MBE calculated with all available observed-modeled pairs in Group 2 for the NDBC stations. Eleven WRF experiments exhibit three statistical metrics with ranges from 1.49–1.76 m/s (RMSE), 1.14–1.39 m/s (MAE), and -0.44–0.27 m/s (MBE). E09 (Shin-Hong "scale-aware" PBL scheme; referred to as the SH scheme) exhibits the best RMSE result, 1.49 m/s. For MAE, E11 (TKE+TKE dissipation rate [epsilon] scheme) produces the lowest value, 1.14 m/s. E05 (MYNN 3rd level) does not show good results in terms of RMSE and MAE. For MBE, E03 notably underestimates the wind speed (MBE: -0.44 m/s) compared to the other experiments. Given the evaluation results, we selected E09 (SH scheme), which is based on YSU (E02) and designed for sub-kilometer transition scales (i.e., 200 m–1 km). Especially notable is that the vertical mixing algorithms for the stable PBL regime and the free atmosphere from the SH scheme are the same as those from the YSU scheme; thus, E09 produces almost identical results in terms of the statistical metrics compared to E02. Three main reasons for the final selection of the SH scheme (E09) for this project are:

- The SH scheme was the only scheme that satisfied RMSE < 1.5 m/s, MAE < 1.2 m/s, and MBE < 0.5 m/s.
- For the evaluation of modeled wind speed at hub height, the SH scheme showed the overall best performance compared to other PBL schemes (not shown in this report).
- Given the complex topography of the island, a higher spatial resolution would be needed (as a future extension of this work). In this case, the SH scheme designed for sub-kilometer transition scales will be useful to efficiently improve the current spatial resolution.

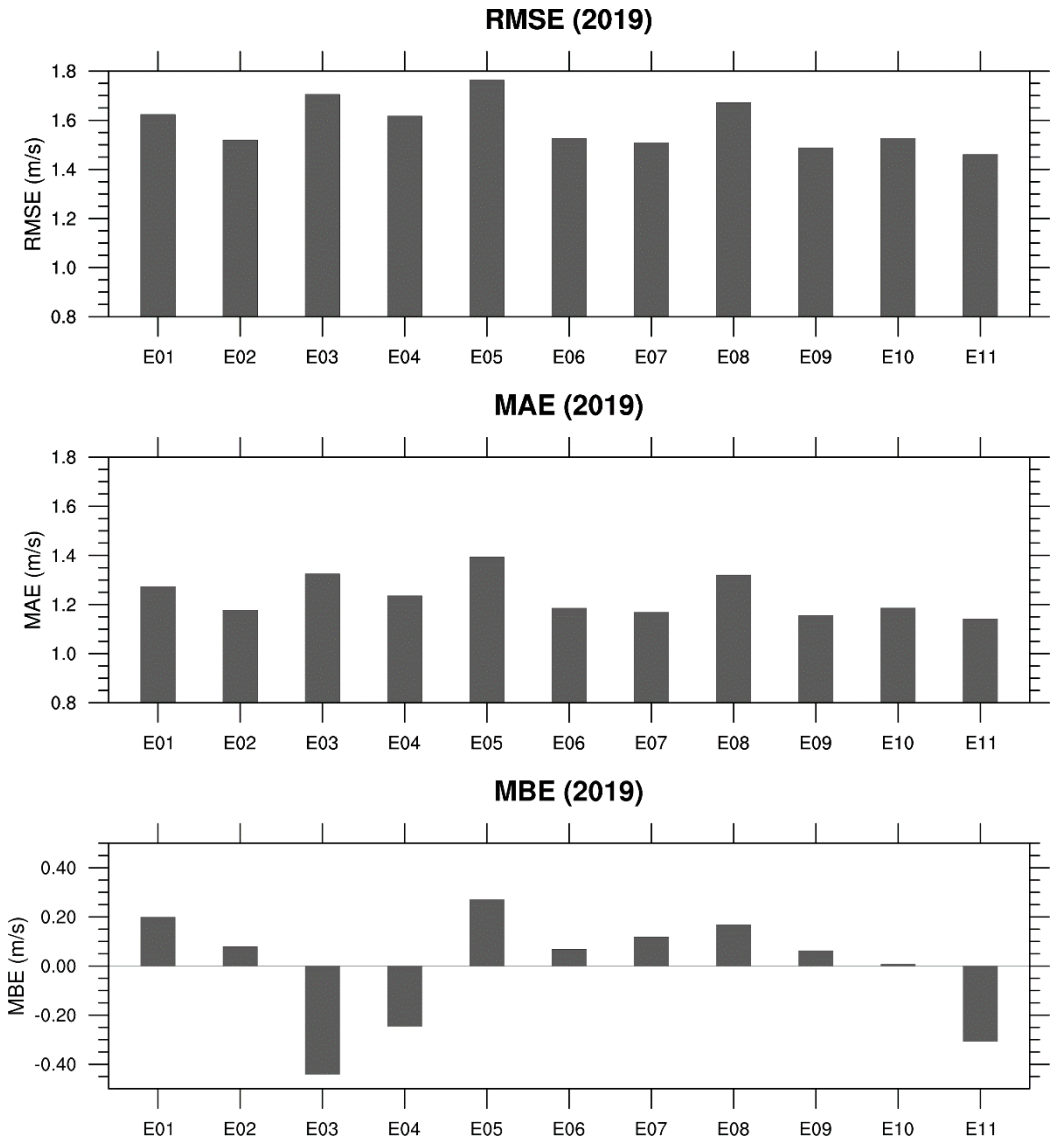

Figure 9. RMSE (m/s), MAE (m/s), and MBE (m/s) of WRF wind speed computed with all available data for NDBC sites (2019)

For Puerto Rico, the wind data covering the years from 2001–2020 were produced by using the SH scheme, which is the final selection for the PBL parameterization from the WRF model.

Comparisons of the surface wind speed from E09 against NDBC data using annual RMSE, MAE, and MBE are presented in Figure 10. For the evaluation of WRF wind speed, we used data from all available NDBC stations for each year from 2006–2020 (Table 4). It appears that Hurricane Maria (September 2017) affected the buoys and resulted in a decrease in observational data availability. The damaged stations need to be repaired to increase data availability to pre-hurricane levels. The annual statistical metrics show reasonable values for RMSE, MAE, and MBE, which are smaller than 2.0 m/s, 1.5 m/s, and ±0.5 m/s, respectively, for all 15 years. In addition, the MBE is approximately within ~8% of the buoy observations across 15 years.

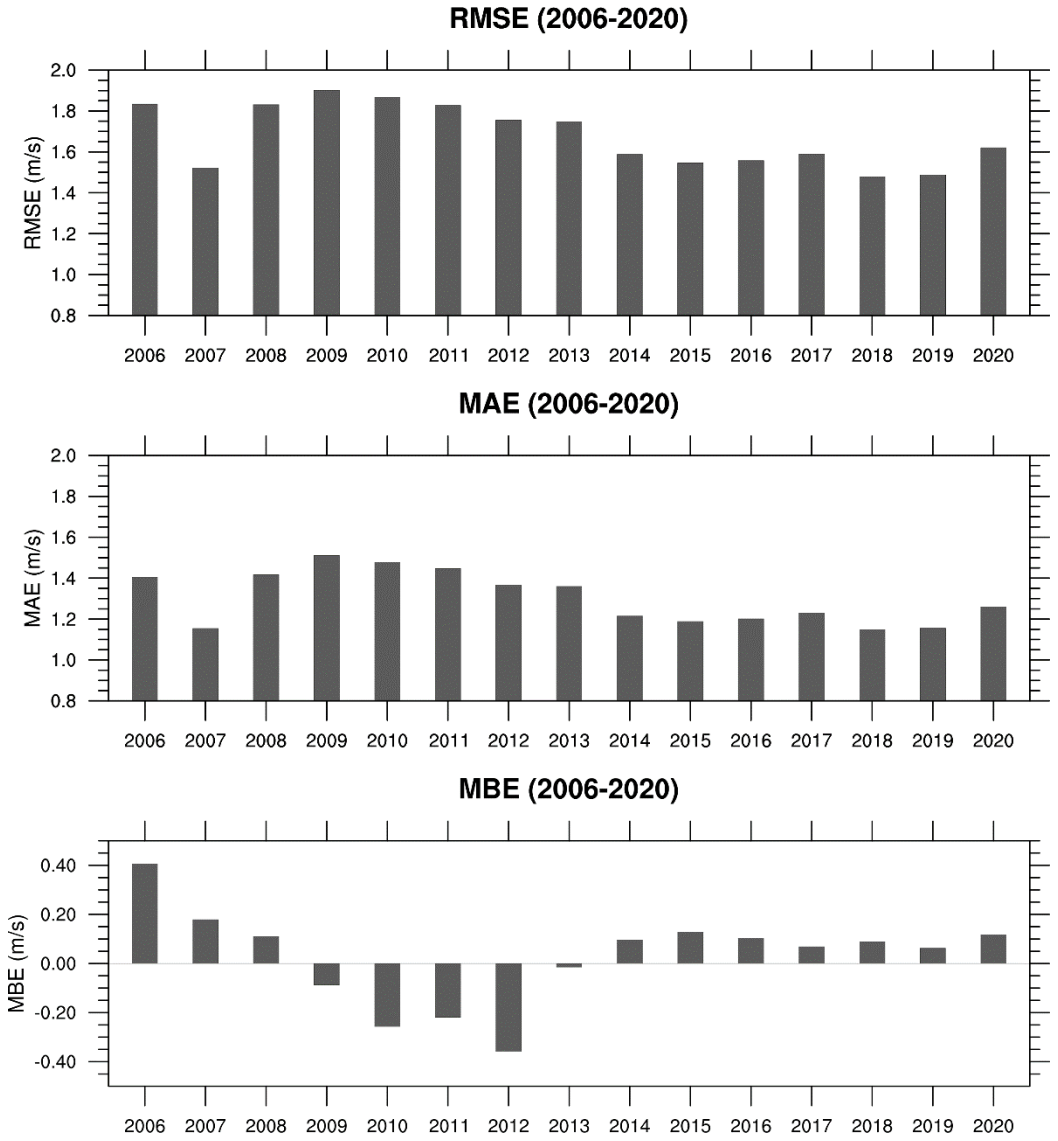

Figure 10. RMSE (m/s), MAE (m/s), and MBE (m/s) of WRF wind speed computed with all available data for NDBC sites (2019)

Table 4. Number of NDBC Stations Available for Each Year (2006–2020)

Year	2006	2007	2008	2009	2010	2011	2012	2013
# of Stations for Data Available	3	3	5	8	15	14	16	18
Year	2014	2015	2016	2017	2018	2019	2020	
# of Stations for Data Available	14	15	14	13	7	8	8	

3.3 Post-Processing of WRF Outputs

For Puerto Rico, we used the WRF to produce the gridded wind resource data covering the years from 2001–2020. To provide a downstream model-friendly format—e.g., for the Renewable Energy Potential (reV) model and System Advisor Model (SAM)—the WRF outputs were postprocessed following the WIND Toolkit format. The WRF outputs processed through the WIND Toolkit include wind profile and basic meteorological variables (Table 5). We processed the 5-minute WRF outputs to generate two postprocessed data sets that have 5-minute and hourly resolutions. The hourly wind resource data served as the basis in analyzing the wind energy cost for Puerto Rico (Duffy et al. 2022).

Table 5. Variables From Postprocessed WRF Outputs (WIND Toolkit Format)

Variable Name	Height (m)	Unit
inversemoninobukhovlength_2m	2	m^{-1}
relativehumidity	2	Percentage
pressure	0,100,200,300	Pa
temperature	2, 10, 20, 60, 80, 100, 120, 140, 160, 180, 200, 220, 240, 260, 280, 300, 400, 500	°C
winddirection	10, 20, 40, 60, 80, 100, 120, 140, 160, 180, 200, 220, 240, 260, 280, 300, 400, 500	Degrees from N
windspeed	10, 20, 40, 60, 80, 100, 120, 140, 160, 180, 200, 220, 240, 260, 280, 300, 400, 500	m/s
surface_sea_temperature		°C
friction_velocity	2	m/s
surface_heat_flux		W/m^2
skin_temperature		°C
boundary_layer_height		M
roughness_length		M
virtual_potential_temperature	2, 10, 20, 40, 60, 80, 100, 120, 140, 160, 180, 200, 220, 240, 260, 280, 300, 400, 500	°C

4 Analysis of the 20-Year Wind Resource Data

The 20-year wind resource data are a feasible source of information to study the measurable strength, temporal and spatial distributions, and temporal and spatial variations of the wind resource in the greater Puerto Rico region.

4.1 An Overview of the Long-Term Wind Resource Data

Figure 11 shows the 20-year mean wind speeds in the greater Puerto Rico region at heights of 10 m, 40 m, 80 m, 120 m, 160 m, and 200 m. Due to the surface friction (roughness) and the resultant wind speed gradient, the average wind velocity generally increases with height over both land and ocean. Over land, the average wind speed increases from approximately 2 m/s to 10 m/s, whereas an evidently reduced wind speed gradient is seen over the ocean. The wind speed over the ocean is significantly higher than over land because of the lower surface friction and therefore lower resistance to the wind flow. Although the land-based and offshore regions in Puerto Rico possess adequate wind resource at the heights of the conventional wind turbines (Figure 11), the island of Puerto Rico can be divided into two major regions according to the strength of the wind resource. The southern area of Cordillera Central and the Sierra de Cayey mountains have substantially higher wind speed on average compared to the northern area due to the different topographic relief and climatology (Gomez-Gomez et al. 2014). At the same height from ground, the LBW speed in the southern area can be even higher than the nearby offshore regions. This is probably caused by the substantially higher altitude in the mountain region. As shown in Figure 12, the island of Puerto Rico is dominated by the prevailing trade winds. The northeast wind leads to the relatively humid climate in the northern area, whereas a much lower rainfall amount is found in the leeward side of the mountains. In the southern area, southeast wind is often found during the daytime, though it is barely discernable in the long-term average of the wind directions, as shown in Figure 12 (Gomez-Gomez et al. 2014).

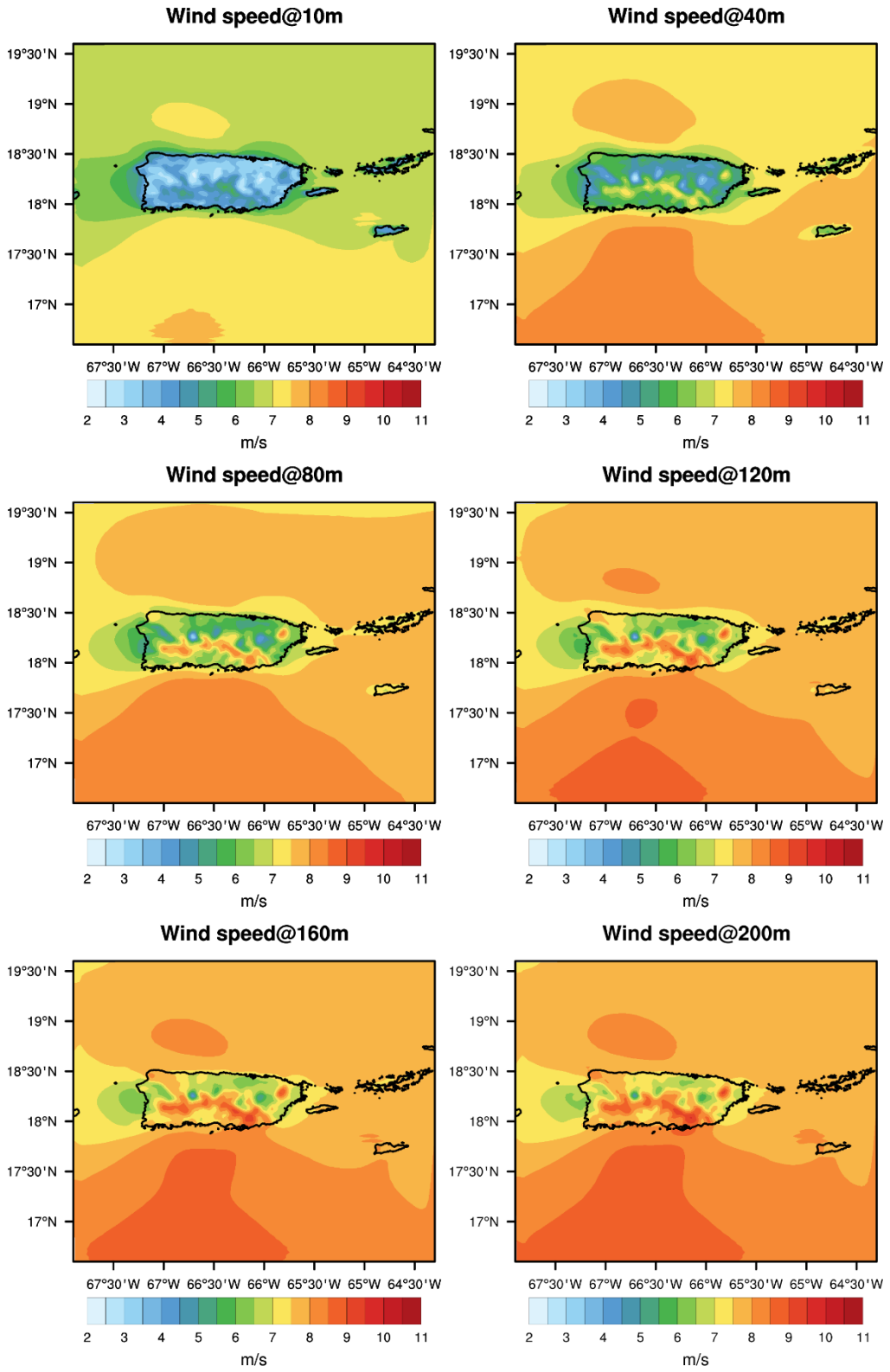

Figure 11. Twenty-year mean wind speeds at different heights

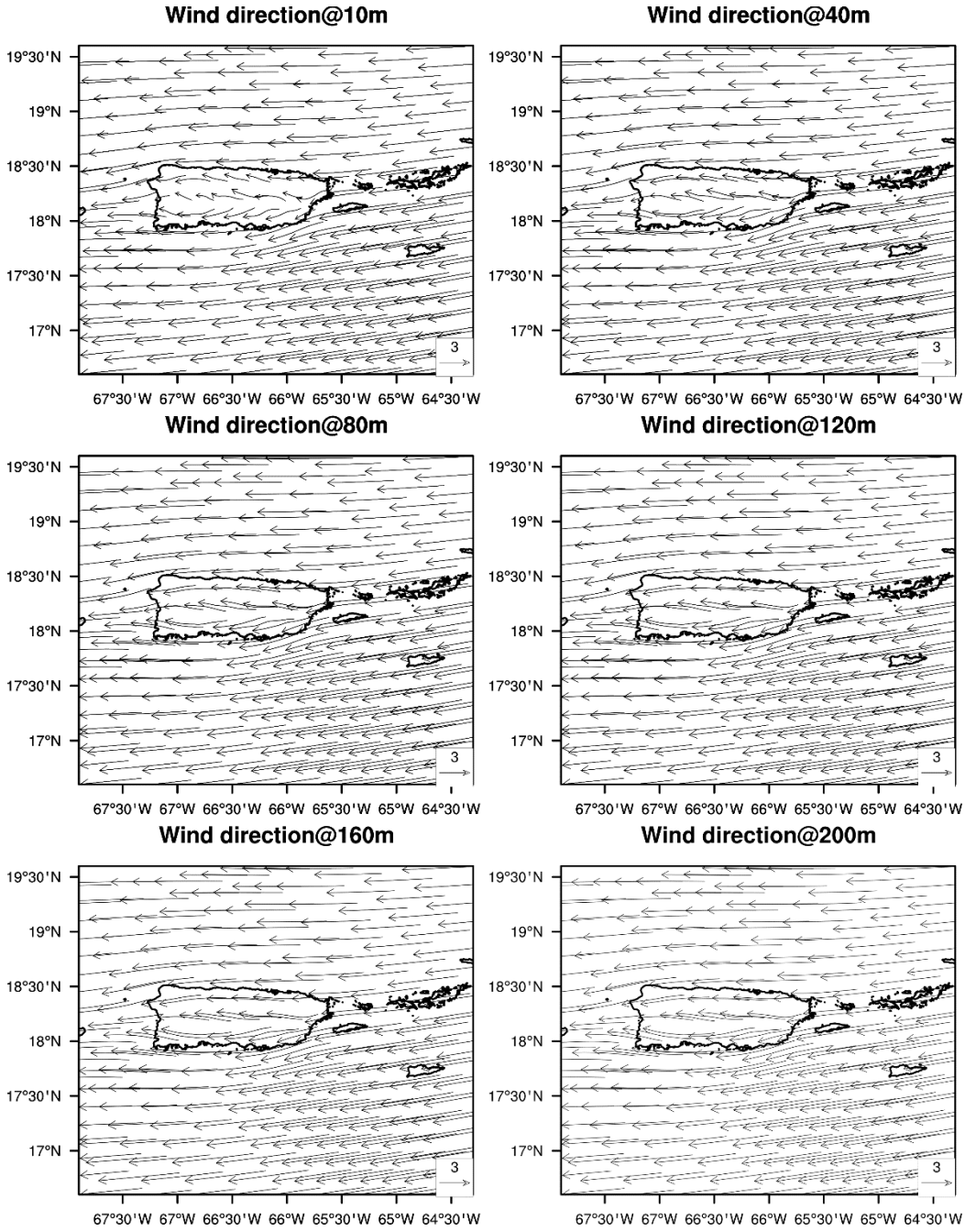

Figure 12. Twenty-year mean wind directions at different heights

4.2 Twenty-Year Data for Selected Land-Based and Offshore Sites

Figure 13 and Figure 14 display the annual mean wind speeds at the offshore and land-based sites, respectively, at a height of 160 m. During the 20 years from 2001–2020, the southeast site has the largest wind speed on average among all the offshore sites because it is affected by both the southeast wind and northeast wind in the daytime and nighttime, respectively. The OSW speeds at the northwest and northeast sites have similar strength because they are mainly affected by the northeast wind. The prevailing trade wind from the northeast is reduced by a prevailing west wind along the western end of Puerto Rico, which is shown in the data of the west site in

Figure 13. As demonstrated in Figure 11, the LBW speed in Puerto Rico is correlated with the altitude of the site. This explains the larger wind speeds in the northwest and southwest sites in Figure 14, where the two sites have higher altitudes than the northeast and southeast sites.

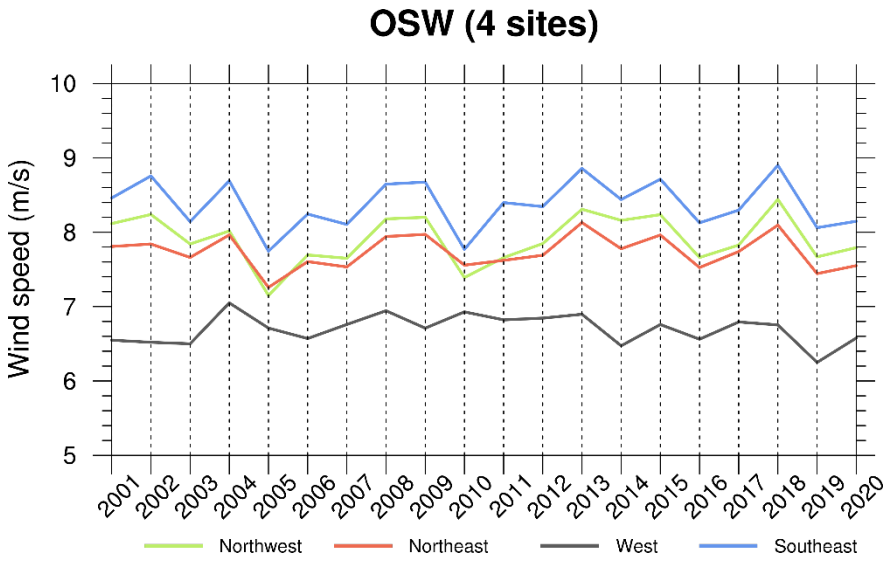

Figure 13. Annual mean OSW at 160 m

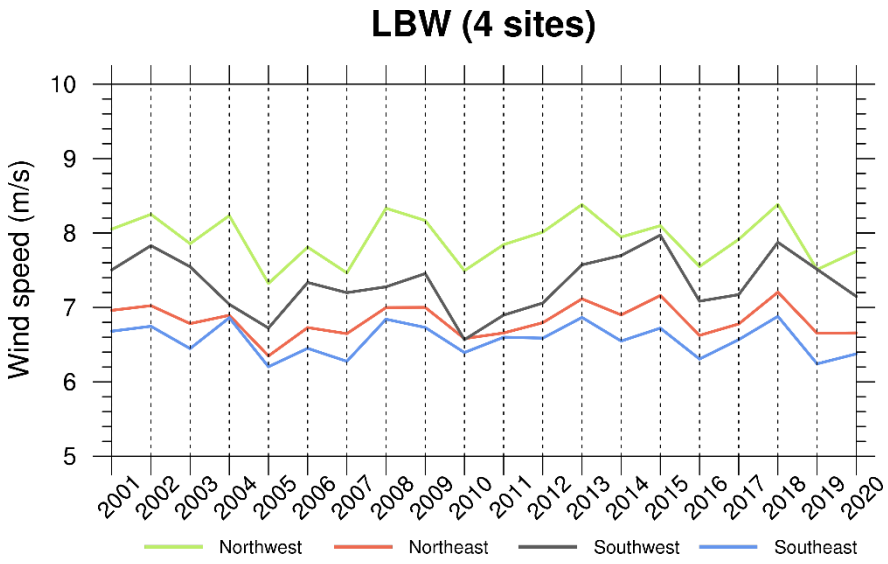

Figure 14. Annual mean LBW at 160 m

Figure 15 and Figure 16 display the monthly mean wind speeds at the offshore and land-based sites, respectively, over 20 years at a height of 160 m. The results show that summer and winter are the seasons with peak wind speeds for most offshore sites, with much lower wind speeds likely to be found in October (Figure 15). In the west site, however, the wind speed for summer is not evidently higher than spring, which might be related to the distinct wind direction. At the land-based sites (Figure 16), the peak wind speed for the southwest site arrives 1 month earlier than the other sites.

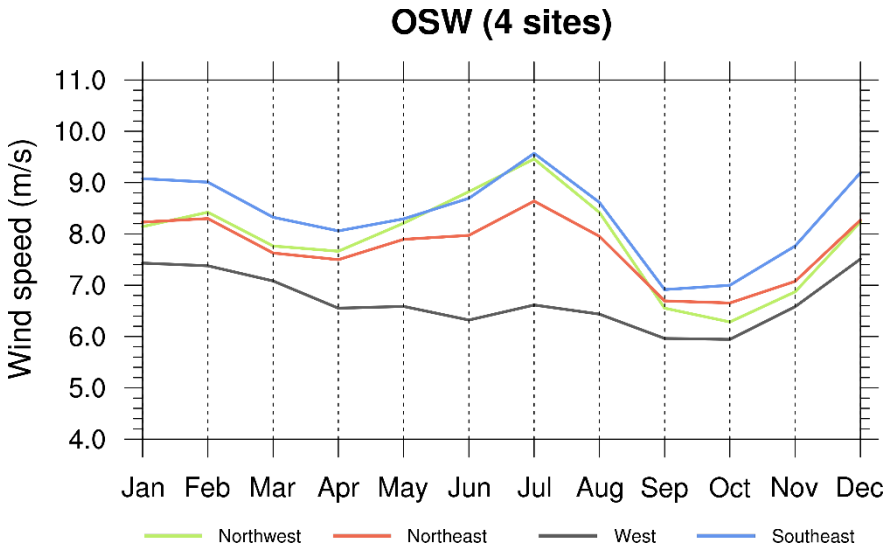

Figure 15. Monthly mean OSW over 20 years at 160 m

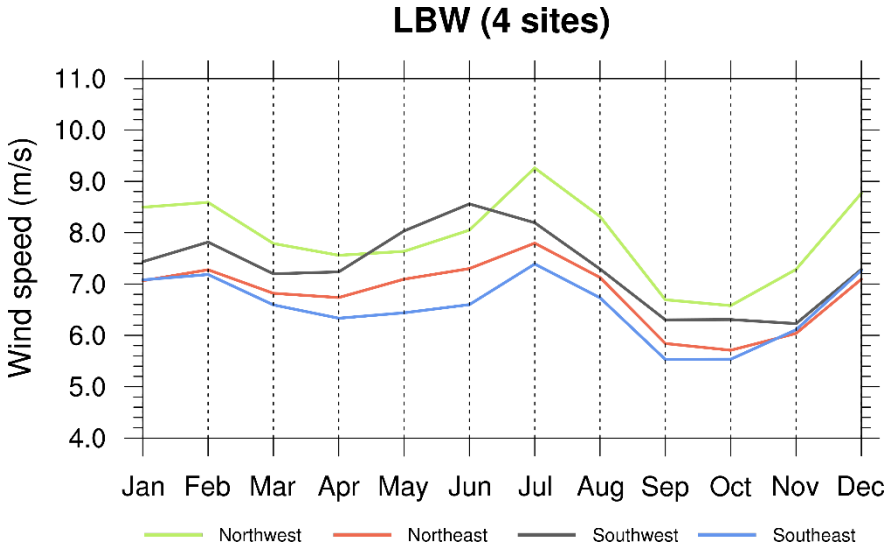

Figure 16. Monthly mean LBW over 20 years at 160 m

Figure 17 illustrates the hourly wind speeds at 160 m for the offshore and land-based sites. The OSW at the northwest site has a strong diurnal variation for all seasons, where the minimum and maximum wind speeds occur in the early morning and early afternoon, respectively. A similar pattern can be found in the LBW for the northeast and southwest sites. Due to the distinct dominant wind direction, the OSW in the west site has the lowest and highest wind speeds around noon and midnight, respectively. The wind speed for the other sites shows insignificant diurnal variation. The distributions of the hourly wind speeds at 160 m for the offshore and land-based sites are shown in Figure 18 and Figure 19, respectively. The results show that the wind speeds in the eastern part of Puerto Rico are symmetrically distributed around the most probable wind speeds. In the western part of Puerto Rico, however, the distribution is asymmetric, with a significantly higher occurrence of low wind speeds than high wind speeds. This is a result of the reduction of the prevailing trade wind when flowing from east to west. The reduction should be more visible at the land surface.

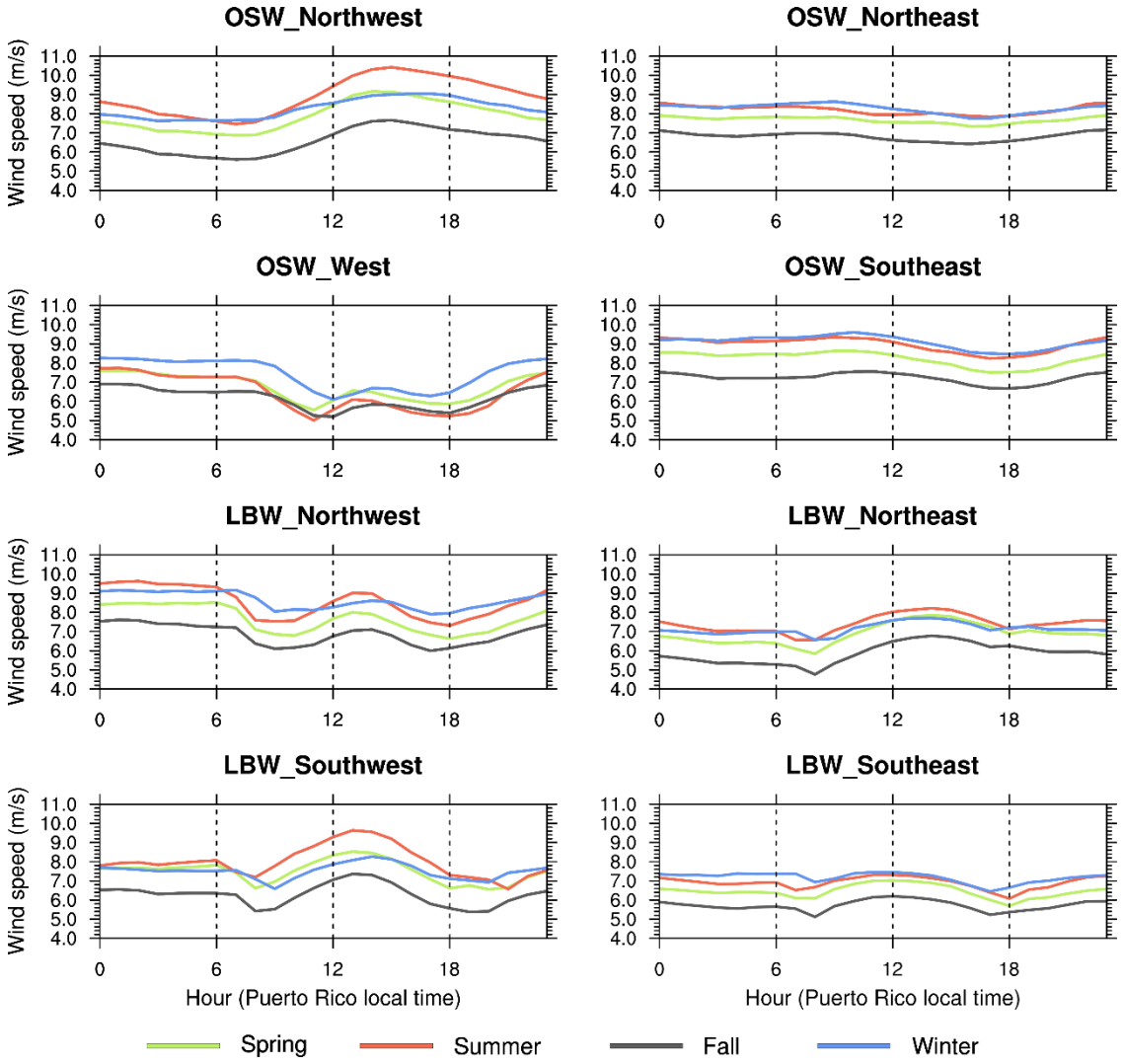

Figure 17. Hourly wind speeds at 160 m for the OSW and LBW sites

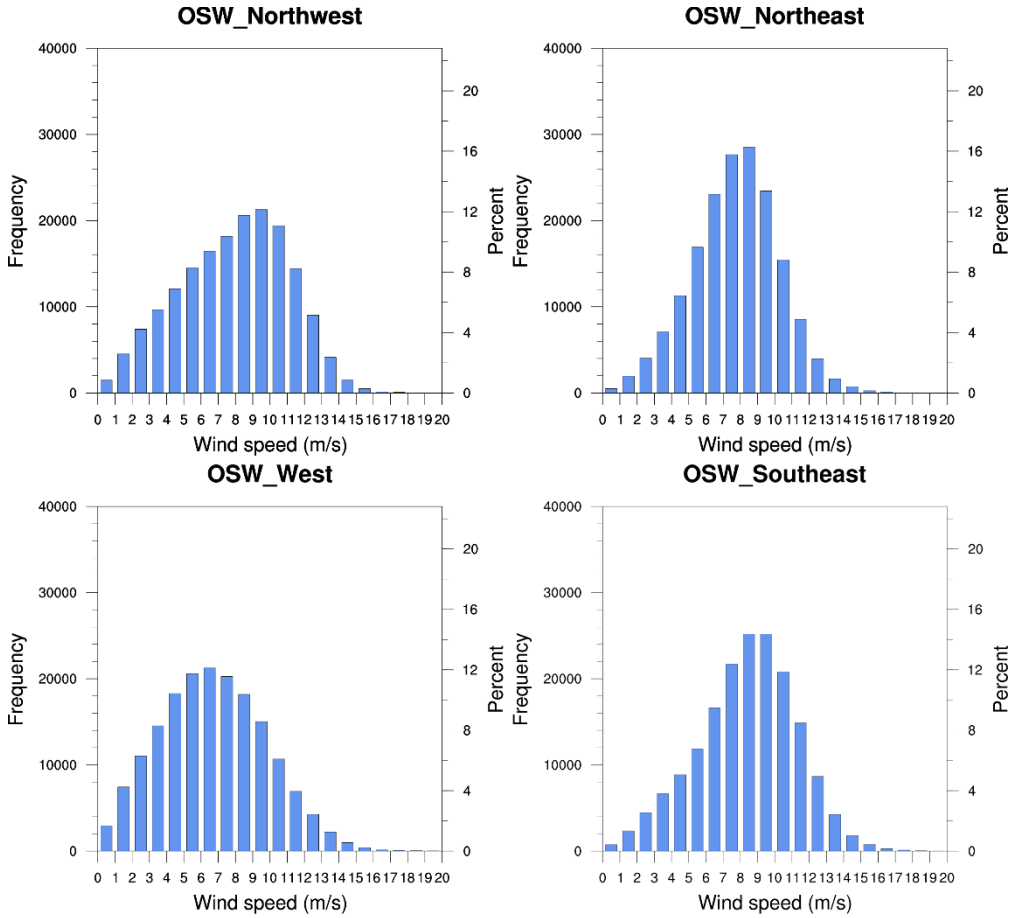

Figure 18. Distribution of hourly OSW for four sites at 160 m

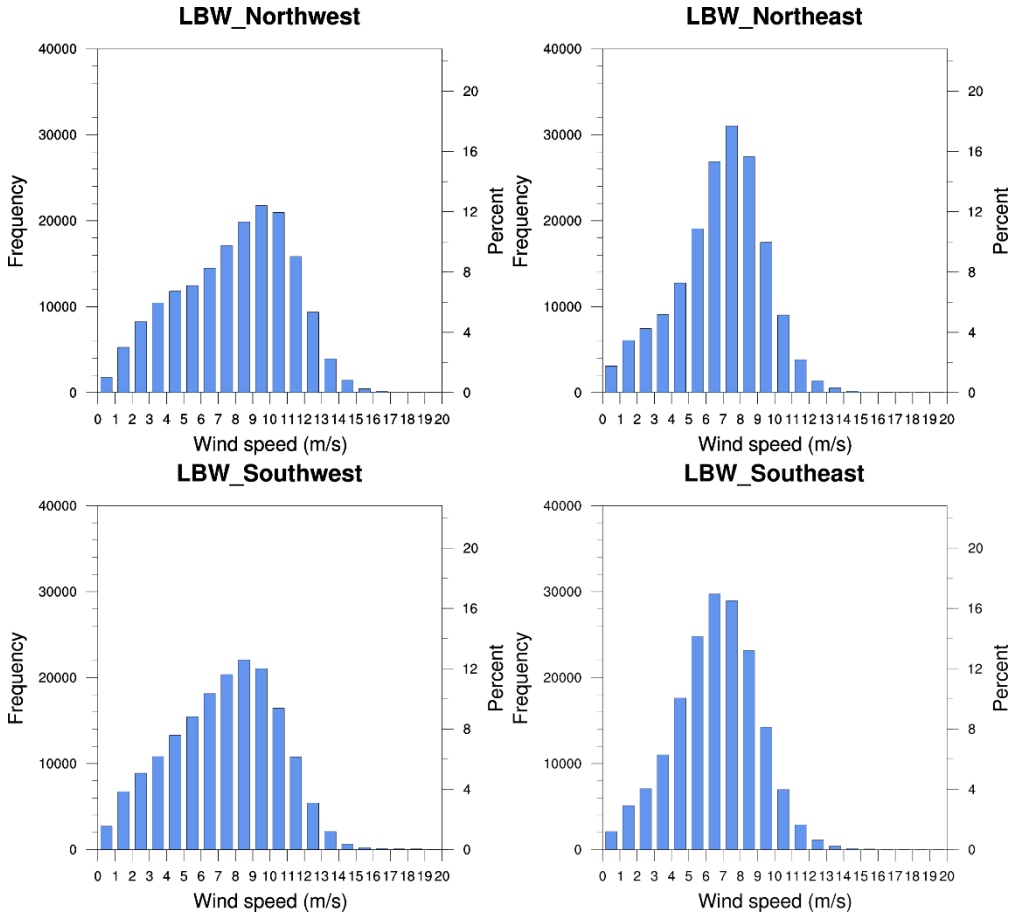

Figure 19. Distribution of hourly LBW for four sites at 160 m

Figure 20 and Figure 21 show the hourly averaged wind speed and wind direction at 160 m for the offshore and land-based sites, respectively. The OSW in the northeast and southeast sites is dominated by easterly and northeasterly wind (Figure 20). The OSW directions are diversely distributed in the western part of Puerto Rico, as shown for the west site. For LBW, the northwest site is dominated by easterly and northeasterly wind, whereas the southwest site is dominated by easterly and southeasterly wind. The LBW in the northeast and southeast sites are from the east, northeast, and southeast.

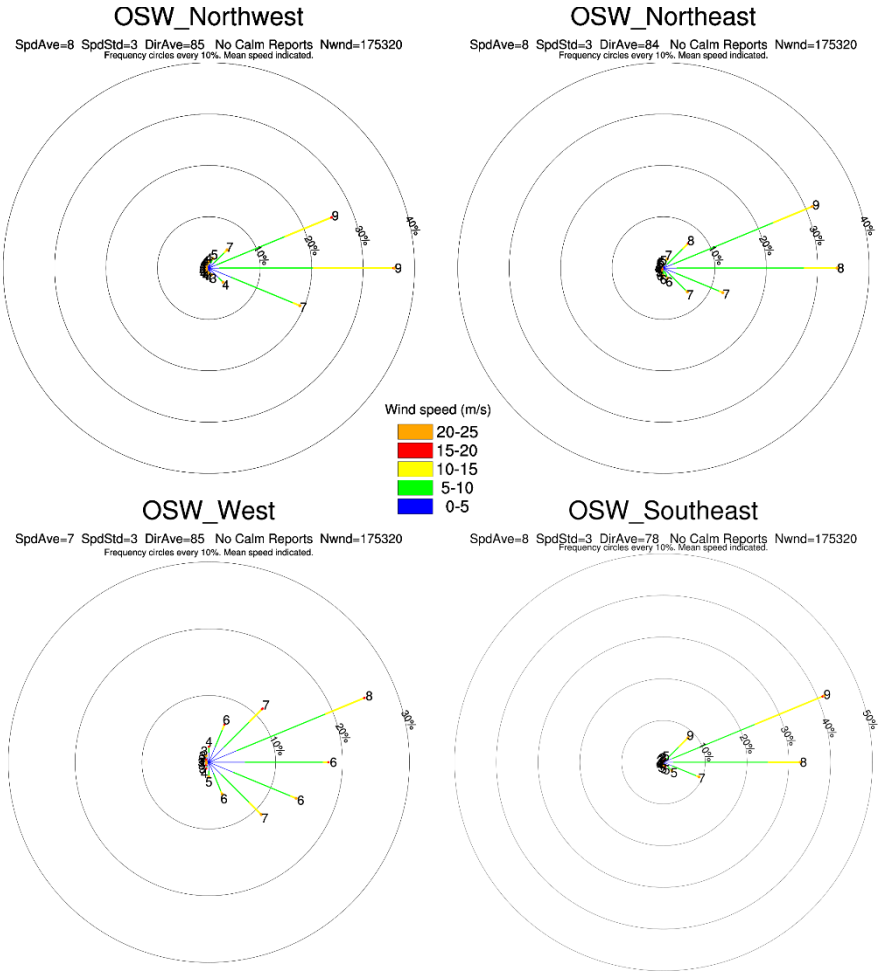

Figure 20. Wind rose diagram for hourly OSW at 160 m

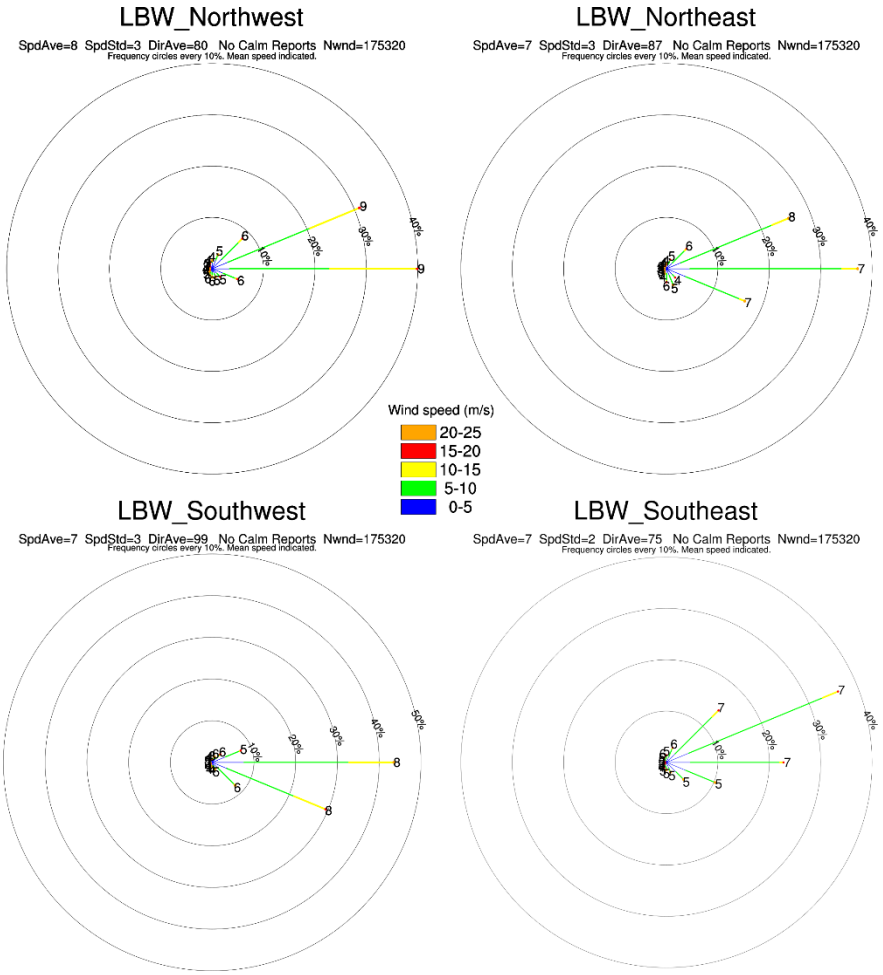

Figure 21. Wind rose diagram for hourly LBW at 160 m

The vertical distributions of the hourly wind speeds at the offshore sites and land-based sites are given in Figure 22 and Figure 23, respectively. From 10 m to 200 m, the OSW speed slightly increases for all four sites (Figure 22). The rate of increase is greatly reduced above 40 m due to the reduced friction in the upper atmosphere. Compared to OSW, the LBW speed rapidly increases with height because of the greater surface roughness of land compared to the ocean (Figure 23).

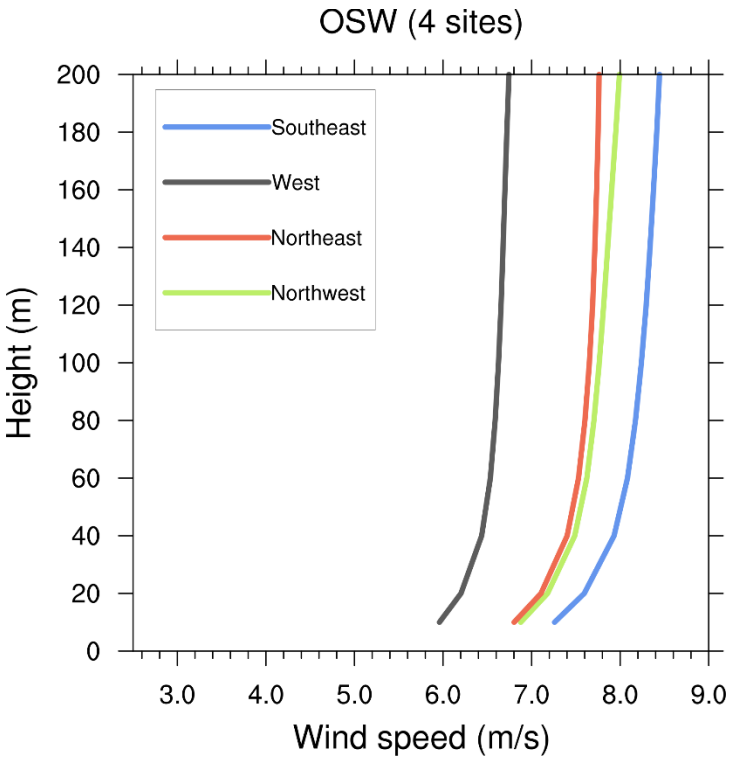

Figure 22. Hourly mean wind profiles for the OSW sites

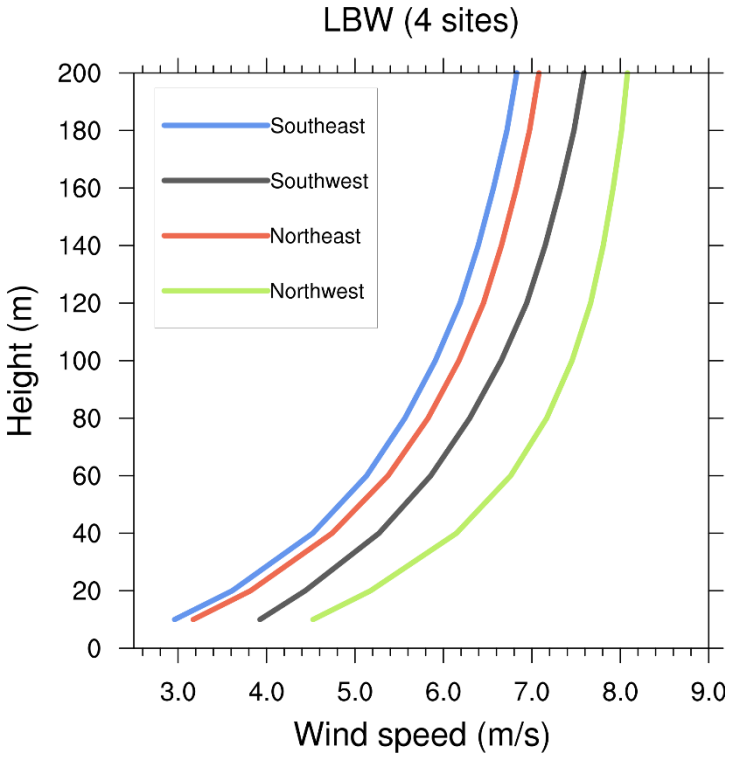

Figure 23. Hourly mean wind profiles for the LBW sites

4.3 Case Study: Hurricane Maria

Hurricane Maria, a tropical cyclone, made landfall in Puerto Rico on September 20, 2017. Maria resulted in significant impacts on the Puerto Rico region, including deaths, injuries, critical infrastructure damages, and significant power network interruptions. This hurricane caused an estimated $90 billion in damages for Puerto Rico, and it was recorded as the third costliest tropical cyclone in the United States since 1900 (Kishore et al. 2018).

Given the devastating effects of hurricanes, the wind data sets that can capture extreme-weather events are important for various studies and applications related to renewable energy. Usually, extreme weather events bring utmost challenges to power system reliability and resilience due to their multifaceted impacts on renewable generation resources, demand, and power system outages. In this section, we briefly analyze the 2017 wind data sets, which include spatiotemporally simulations of Hurricane Maria.

Figure 24 displays the best track from the National Hurricane Center (Pasch, Penny, and Berg 2019) and the modeled track from WRF for Hurricane Maria. For WRF, the hurricane track was calculated from the minimum sea level pressure. The WRF tracked Maria slightly differently to the National Hurricane Center record when the storm was approaching the island and very close to observations after it made landfall.

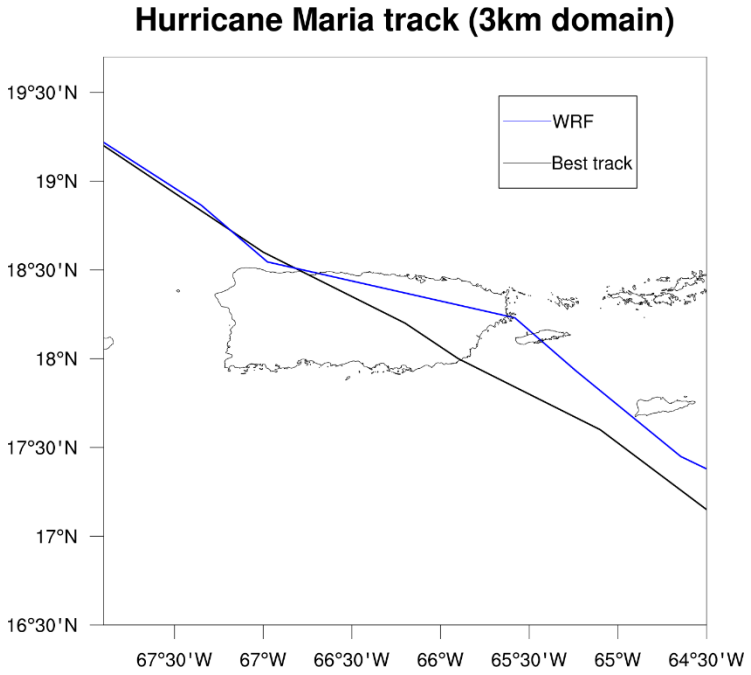

Figure 24. Hurricane track representing minimum sea level pressure (black: best track, blue: WRF)

Figure 25 shows the simulated 160-m wind speed and wind direction for Hurricane Maria from the WRF model. Maria made landfall in southeastern Puerto Rico in the morning hours of September 20, 2017. When making landfall, Maria was a Category 4 hurricane (Pokhrel et al. 2021). The official landfall time of Maria in Puerto Rico (i.e., Maria's center crossing the southeast coast of Puerto Rico near Yabucoa) (Pasch, Penny, and Berg 2019) was 10:15 UTC September 20, 2017. Even though the WRF, using our selected physics configuration, does not perfectly capture the landfall time and location compared with the best track (from the point of

view of the minimum sea level pressure), it produces modeled wind demonstrating that Puerto Rico was under the influence of Hurricane Maria (Figure 25). According to the National Hurricane Center record, the center of Hurricane Maria crossed the island diagonally from southeast to northwest for several hours; and then emerged into the Atlantic around 18:00 UTC September 20, 2017. WRF captured the time and location of those scenes in representing Hurricane Maria, as shown in Figure 24 and Figure 25. The center of Maria's circulation exited Puerto Rico around 06:00 UTC September 21, 2017.

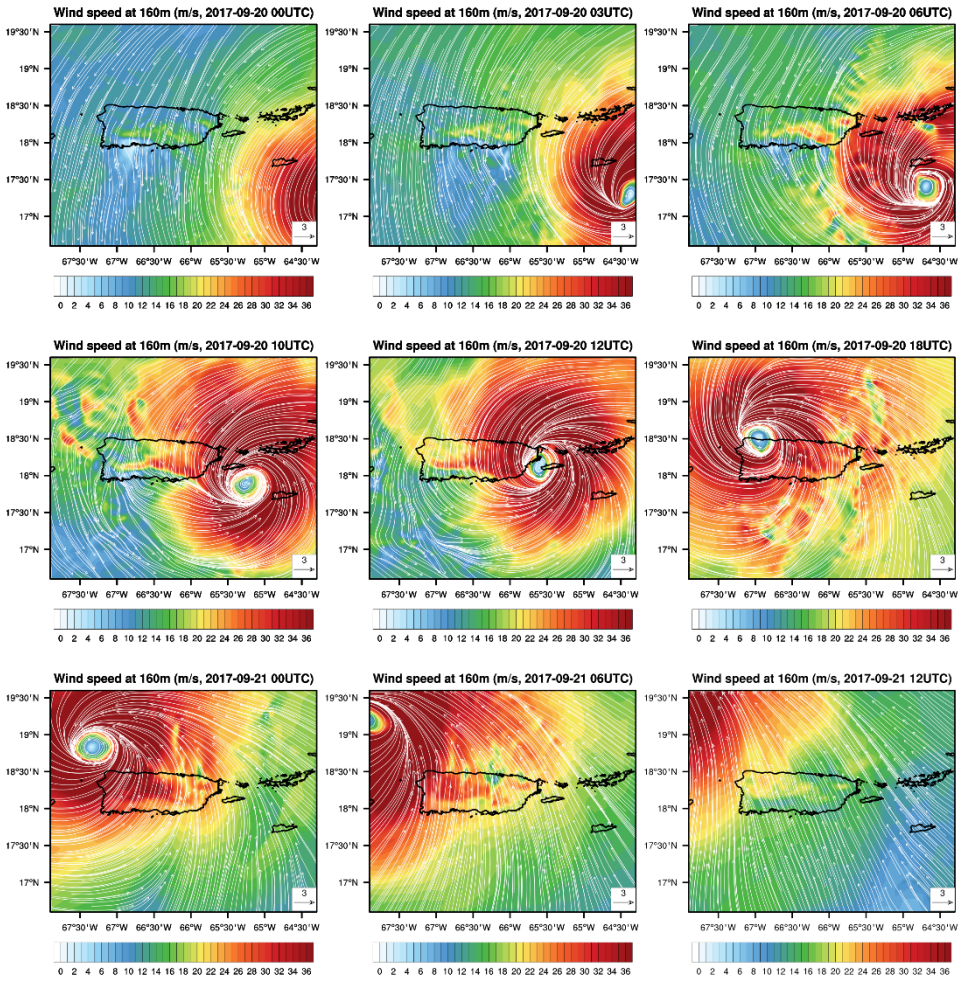

Figure 25. Two-dimensional maps of 160-m wind speed and wind direction for Hurricane Maria simulated from WRF (00 UTC 09/20/2017–12 UTC 09/21/2017)

For the OSW and LBW sites, we analyzed the time series of 160-m wind speed during Hurricane Maria (Figure 26 and Figure 27). For OSW, the northeast site shows the peak wind speed at 12 UTC September 20, 2017, which is earlier than other locations (Figure 26), because of Maria's landfall on the southeastern side of Puerto Rico (see magnitude of wind speeds in Figure 26). The southeast sites exhibit lower wind speed than other locations because this site was not exposed to Maria's highest winds. For the site in the northwest, the wind speed suddenly dropped at 16 UTC September 20, 2017. This is because at that time the site was in the hurricane's eyewall, where low wind speeds occurred (see Figure 26). During Hurricane Maria,

the magnitude of OSW ranged from 10.3–45.2 m/s, 14.7–55.2 m/s, 10.5–48.7 m/s, and 4.9–32.9 m/s for the northwest, northeast, west, and southeast sites, respectively.

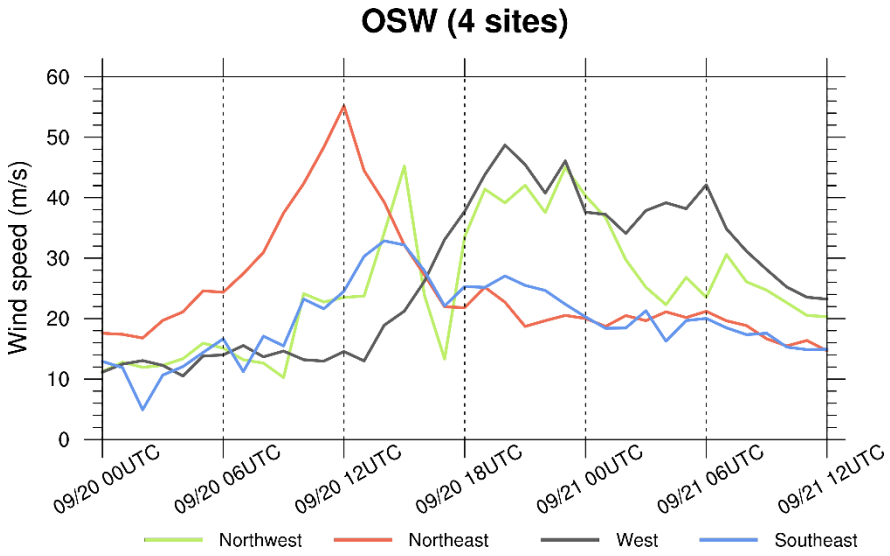

Figure 26. Time series of 160-m wind speed during Hurricane Maria for OSW sites (00 UTC 09/20/2017–12 UTC 09/21/2017)

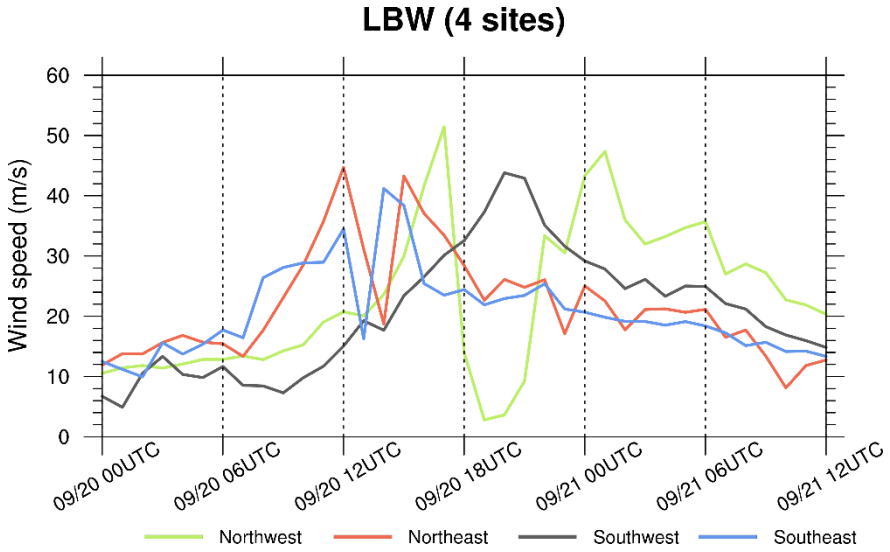

Figure 27. Time series of 160-m wind speed during Hurricane Maria for OSW sites (00 UTC 09/20/2017–12 UTC 09/21/2017)

Figure 27 shows the time series of the 160-m wind speed for the LBW sites. For LBW, the sites in the northeast and southeast show similar patterns for time series of wind speed because the two sites were located within the track of Maria (e.g., a sudden decrease in wind speed at a similar time when the eyewall passed). The LBW at the northwest site exhibited a notable decrease from 51.4 m/s to 2.8 m/s at 18 UTC September 20, 2017, because the center of hurricane passed the location. During Hurricane Maria, the magnitude of LBW ranged from 2.8–51.4 m/s, 8.1–44.7 m/s, 4.9–43.8 m/s, and 10.0–41.2 m/s for the northwest, northeast, southwest, and southeast sites, respectively.

For the OSW and LBW sites, we analyzed the wind profile during Hurricane Maria (Figure 28 and Figure 29). The 20 years of averaged wind profiles for the OSW sites show wind speeds ranging from 5.5–8.5 m/s (see Figure 22). On the other hand, the wind speeds are distributed from 9–18 m/s for the various heights (10–200 m) when Hurricane Maria was approaching Puerto Rico (00:00 UTC September 20, 2017) (Figure 28). Very strong winds that are greater than 30 m/s were captured during Maria, especially at the OSW site in the northeast, where the magnitude of the wind speeds for the vertical profile ranged from 42–56 m/s at 00:00 UTC September 20, 2017 (Figure 28), because the location was under the strong influence of the hurricane (see Figure 25).

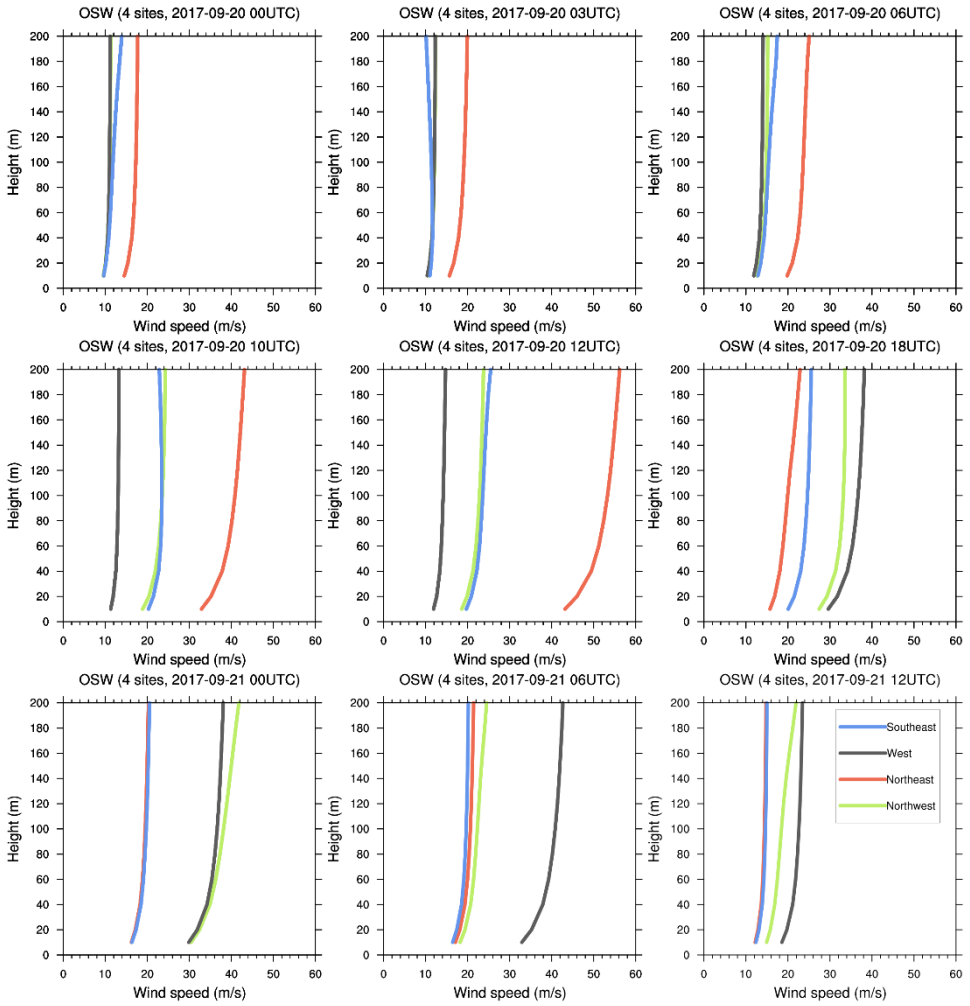

Figure 28. Wind profiles for OSW sites during Hurricane Maria (00 UTC 09/20/2017–12 UTC 09/21/2017)

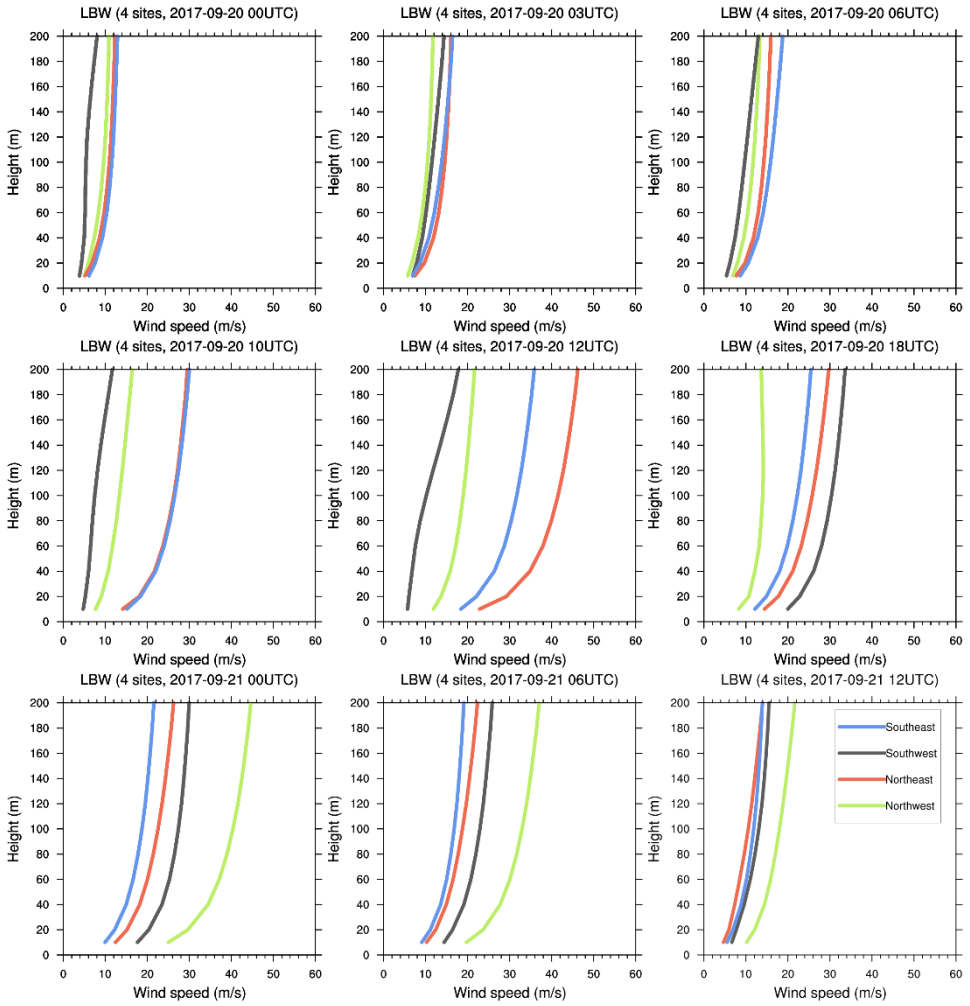

Figure 29. Wind profiles for LBW sites during Hurricane Maria (00 UTC 09/20/2017–12 UTC 09/21/2017)

For the LBW sites, the 20 years of mean wind profiles exhibit wind speeds ranging from 2.8–8.2 m/s for heights from 10–200 m (see Figure 23). When the hurricane was approaching the island (00:00 UTC September 20, 2017, in Figure 29), the LBW sites showed a lower magnitude of wind speeds in their wind profiles than the OSW profiles (Figure 28). Very high wind speeds (>30 m/s) are also captured in LBW sites during the passage of the hurricane (see Figure 25). The northeast site shows wind speed magnitudes ranging from 22–46 m/s at 00:00 UTC September 20, 2017 (Figure 29). Even though the locations of the northeast sites for LBW and OSW are under almost identical influence of the hurricane (i.e., given the wind magnitude and wind circulation at 00:00 UTC September 20, 2017, shown in Figure 25), the LBW profile shows higher wind speeds than the OSW profile.

5 Summary

This report presents the development of 20 years of wind resource data sets for Puerto Rico. The main research steps in developing the long-term data sets include (1) modeling the wind resource using an NWP model, (2) development and validation of the wind resource data sets, and (3) analysis of the 20 years of wind resource data for the Puerto Rico region.

The major achievements and findings in (1), (2), and (3), are:

1. The WRF model (Version 4.3) was used to dynamically downscale the ERA5 reanalysis data (0.25°×0.25°; hourly interval) to a 3-km WRF grid, which covers Puerto Rico and the U.S. Virgin Islands. WRF simulations were implemented for each month, and then we stitched 12 sets of the 1-month simulation in a postprocessing step to generate a year of consecutive data. A spectral nudging technique was applied to prevent the WRF model from departing from its boundary conditions when running 1-month simulations.
2. WRF configurations using 11 different PBL parameterizations were tested to select the right combination of physics that can provide accurately modeled wind speeds for Puerto Rico. Through an evaluation of the model output resulting from the 11 PBL physics schemes against observations obtained from the NDBC and at hub height for a location for which data were available, the Shin-Hong PBL scheme was selected to generate the 20 years of wind resource data (3-km and 5-minute for the spatial and temporal resolutions, respectively) for Puerto Rico.
3. The modeled 20 years of wind data sets were analyzed for land-based and offshore sites.

The WRF output was postprocessed to include wind profiles and basic meteorological variables in a format that can be easily used as input by other models. The wind resource data sets will be made publicly available through NREL. The data sets developed in this project will be primarily used for wind energy development considerations for the Puerto Rico Grid Resilience and Transition to 100% Renewable Energy Study (PR100).

References

Al-Yahyai, S., Y. Charabi, and A. Gastli. 2012. "Review of the Use of Numerical Weather Prediction (NWP) Models for Wind Energy Assessment." *Renewable and Sustainable Energy Reviews* 14: 3192–3198.

Bañuelos-Ruedas, F., C. Camacho, and S. Rios-Marcuello. 2011. "Methodologies Used in the Extrapolation of Wind Speed Data at Different Heights and its Impact in the Wind Energy Resource Assessment in a Region." Wind Farm—Technical Regulations, Potential Estimation and Siting Assessment.

Chen, F., and J. Dudhia. 2001. "Coupling an Advanced Land Surface—Hydrology Model with the Penn State—NCAR MM5 Modeling System. Part I: Model Implementation and Sensitivity." *Monthly Weather Review* 129: 569–585.

Christiansen, M. B., W. Koch, J. Horstmann, C. B. Bayhasager, and M. Nielsen. 2006. "Wind Resource Assessment from C-Band SAR." *Remote Sensing of Environment* 105: 68–81.

Clough, S., M. Shephard, E. Mlawer, J. Delamere, M. Iacono, K. Cady-Pereira, S. Boukabara, and P. Brown. 2005. "Atmospheric Radiative Transfer Modeling: A Summary of the AER Codes." *Journal of Quantitative Spectroscopy and Radiative Transfer* 91, 233–244.

Coantic, M., and B. Seguin. 1971. "On the Interaction of Turbulent and Radiative Transfers in the Surface Layer." *Boundary-Layer Meteorology* 1: 245–263.

DOE. 2018. *Energy Resilience Solutions for the Puerto Rico Grid*. Washington, D.C.

Draxl, C., A. Clifton, B. Hodge, and J. McCaa. 2015. "The Wind Integration National Dataset (WIND) Toolkit." *Applied Energy* 151: 355–366.

Duffy, P., G.R. Zuckerman, T. Williams, A. Key, L.A. Martinez-Tossas, O. Roberts, N. Choquette, J. Yang, H. Sky, and N. Blair. 2022. *Wind Energy Costs in Puerto Rico Through 2035*. Golden, CO: National Renewable Energy Laboratory.

Dvorak, M., C. Archer, and M. Jacobson. 2009. "California Offshore Wind Energy Potential." *Renewable Energy* 35: 1244–1254.

Ferrier, B., Y. Jin, Y. Lin, T. Black, E. Rogers, and G. DiMego. 2002. "Implementation of a New Grid-Scale Cloud and Precipitation Scheme in the NCEP Eta Model."

Gadad, S., and P. Deka. 2016. "Offshore Wind Power Resource Assessment Using Oceansat-2 Scatterometer Data at a Regional Scale." *Applied Energy* 176: 157–170.

Gelaro, R., W. McCarty, M. Suárez, R. Todling, A. Molod, L. Takacs, C. Randles, A. Darmenov, M. Bosilovich, R. Reichle, and K. Wargan. 2017. "The modern-era retrospective analysis for research and applications, version 2 (MERRA-2)." *Journal of Climate* 30, 5419–5454.

Gómez, B., and G. Miguez-Macho. 2017. "The Impact of Wave Number Selection and Spin-Up Time in Spectral Nudging." *Quarterly Journal of the Royal Meteorological Society* 143: 1772–1786.

Gomez-Gomez, F., J. Rodriguez-Martinez, and M. Santiago. 2014. "Hydrogeology of Puerto Rico and the Outlying Islands of Vieques, Culebra, and Mona," in: Survey, U.S.G. (Ed.). Reston, VA.

Hahmann, A., C. Vincent, A. Peña, J. Lange, and C. Hasager. 2015. "Wind Climate Estimation Using WRF Model Output: Method and Model Sensitivities Over the Sea." *International Journal of Climatology* 35: 3422–3439.

Hasager, C., M. Nielsen, P. Astrup, R. Barthelmie, E. Dellwik, N. Jensen, B. Jorgensen, S. Pryor, O. Rathmann, and B. Furevik. 2005. "Offshore Wind Resource Estimation from Satellite SAR Wind Field Maps." *Wind Energy* 8: 403–419.

Hersbach, H., B. Bell, P. Berrisford, S. Hirahara, A. Horányi, J. Muñoz-Sabater, J. Nicolas, C. Peubey, R. Radu, D. Schepers, and A. Simmons. 2020. "The ERA5 Global Reanalysis." *Quarterly Journal of the Royal Meteorological Society* 146: 1999–2049.

Hong, S., Y. Noh, and J. Dudhia. 2006. "A New Vertical Diffusion Package with an Explicit Treatment of Entrainment Processes." *Monthly Weather Review* 134: 2318–2341.

Jimenez, P., and J. Dudhia. 2012. "Improving the Representation of Resolved and Unresolved Topographic Effects on Surface Wind in the WRF Model." *Journal of Applied Meteorology and Climatology* 51: 300–316.

Jiménez, P., J. Dudhia, J. González-Rouco, J. Navarro, J. Montávez, and E. García-Bustamante. 2012. "A Revised Scheme for the WRF Surface Layer Formulation." *Monthly Weather Review* 140: 898–918.

Jimenez, P., J. Yang, J. Kim, M. Sengupta, and J. Dudhia. 2022. "Assessing the WRF-Solar Model Performance Using Satellite-Derived Irradiance from the National Solar Radiation Database." *Journal of Applied Meteorology* 61: 129–142.

Kain, J. S. 2004. "The Kain–Fritsch Convective Parameterization: An Update." *Journal of Applied Meteorology*, 43(1), 170–181.

Kim, J., P. Munoz, M. Sengupta, J. Yang, J. Dudhia, S. Alessandrini, and Y. Xie. 2021. "The WRF-Solar Ensemble Prediction System to Provide Solar Irradiance Probabilistic Forecasts." *IEEE Journal of Photovoltaics* 12. https://doi.org/10.1109/JPHOTOV.2021.3117904.

Kishore, N., D. Marqués, A. Mahmud, M. Kiang, I. Rodriguez, A. Fuller, P. Ebner, C. Sorensen, F. Racy, J. Lemery, and L. Maas. 2018. "Mortality in Puerto Rico After Hurricane Maria." *New England Journal of Medicine* 379: 162–170.

Lu, D., and C. Alcantara. 2017. "After Hurricane Maria, Puerto Rico Was in the Dark for 181 Days, 6 Hours, and 45 minutes." *The Washington Post*.

Miguez-Macho, G., G. Stenchikov, and A. Robock. 2005. "Regional Climate Simulations Over North America: Interaction of Local Processes with Improved Large-Scale Flow." *Journal of Climate* 18: 1227–1246.

Miguez-Macho, G., G. Stenchikov, and A. Robock. 2004. "Spectral Nudging to Eliminate the Effects of Domain Position and Geometry in Regional Climate Model Simulations." *Journal of Geophysical Research* 109.

Mlawer, E., S. Taubman, P. Brown, M. Iacono, and S. Clough. 1997. "Radiative Transfer for Inhomogeneous Atmospheres: RRTM, A Validated Correlated-k Model for the Longwave." *Journal of Geophysical Research: Atmospheres* 102: 16663–16682.

Niu, G., Y. Yang, K. Mitchell, F. Chen, M. Ek, M. Barlage, A. Kumar, K. Manning, D. Niyogi, E. Rosero, M. Tewari, and Y. Xia. 2011. "The Community Noah Land Surface Model with Multiparameterization Options (Noah-MP): 1. Model Description and Evaluation with Local-Scale Measurements." *Journal of Geographical Research* 116: https://doi.org/10.1029/2010JD015139.

Olsen, B., A. Hahmann, A. Sempreviva, J. Badger, and H. Jørgensen. 2017. "An Intercomparison of Mesoscale Models at Simple Sites for Wind Energy Applications." *Wind Energy Science* 2, 211–228.

Optis, M., O. Rybchuk, N. Bodini, M. Rossol, and W. Musial. 2020. *Offshore Wind Resource Assessment for the California Pacific Outer Continental Shelf*. Golden, CO: National Renewable Energy Laboratory.

Pasch, R., A. Penny, and R. Berg. 2019. *National Hurricane Center Tropical Cyclone Report: Hurricane Maria (AL152017)*.

Pokhrel, R., S. del Cos, J. Rincon, E. Glenn, and J. González. 2021. "Observation and Modeling of Hurricane Maria for Damage Assessment." *Weather and Climate Extremes* 33.

Sengupta, M., P. Jimenez, J. Kim, J. Yang, and Y. Xie. 2022. *Final Report on Probabilistic Cloud Optimized Day-Ahead Forecasting System Based on WRF-Solar*. Golden, CO: National Renewable Energy Laboratory.

Sengupta, M., Y. Xie, A. Lopez, A. Habte, G. Maclaurin, and J. Shelby. 2018. *The National Solar Radiation Data Base (NSRDB)*. *Renewable and Sustainable Energy Reviews* 89: 51–60.

Shin, H., and S. Hong. 2015. "Representation of the Subgrid-Scale Turbulent Transport in Convective Boundary Layers at Gray-Zone Resolutions." *Monthly Weather Review* 143: 250–271.

Siuta, D., G. West, and R. Stull. 2017. "WRF Hub-Height Wind Forecast Sensitivity to PBL Scheme, Grid Length, and Initial Condition Choice in Complex Terrain." *Weather and Forecasting* 32: 493–509.

Skamarock, W., J. Klemp, J. Dudhia, D. Gill, Z. Liu, J. Berner, W. Wang, J. Powers, M. Duda, D. Barker, and X. Huang. 2019. *A Description of the Advanced Research WRF Model Version 4*. Boulder, CO: National Center for Atmospheric Research.

Xie, Y., and M. Sengupta. 2018. "A Fast All-Sky Radiation Model for Solar Applications with Narrowband Irradiances on Tilted surfaces (FARMS-NIT): Part I. The Clear-Sky Model." *Solar Energy* 174: 691–702.

Xie, Y., M. Sengupta, and J. Dudhia. 2016. "A Fast All-Sky Radiation Model for Solar Applications (FARMS): Algorithm and Performance Evaluation." *Solar Energy* 135: 435–445.

Xie, Y., M. Sengupta, Y. Liu, H. Long, Q. Min, W. Liu, and A. Habte. 2020. "A Physics-Based DNI Model Assessing All-Sky Circumsolar Radiation." *iScience* 22. doi.org/10.1016/j.isci.2020.100893.

Xie, Y., M. Sengupta, and C. Wang. 2019. "A Fast All-sky Radiation Model for Solar Applications with Narrowband Irradiances on Tilted Surfaces (FARMS-NIT): Part II. The Cloudy-Sky Model." *Solar Energy* 188: 799–812.

Xie, Y., J. Yang, M. Sengupta, Y. Liu, and X. Zhou. 2022. "Improving the Prediction of DNI with Physics-Based Representation of All-Sky Circumsolar Radiation." *Solar Energy* 231: 758–766.

Yang, J., J. Kim, P. Jimenez, M. Sengupta, J. Dudhia, Y. Xie, A. Golnas, and R. Giering. 2021. "An Efficient Method to Identify Uncertainties of WRF-Solar Variables in Forecasting Solar Irradiance Using a Tangent Linear Sensitivity Analysis." *Solar Energy* 220: 509–522.

Yang, J., M. Sengupta, P. Jimenez, J. Kim, and Y. Xie. 2022. "Evaluating WRF-Solar EPS Cloud Mask Forecast Using the NSRDB." *Solar Energy* 243: 348–360.

Zhang, L., J. Xin, Y. Yin, W. Chang, M. Xue, D. Jia, and Y. Ma. 2021. "Understanding the Major Impact of Planetary Boundary Layer Schemes on Simulation of Vertical Wind Structure." *Atmosphere* 12: 777.